


EphrinB2/EphB4 signaling regulates non-sprouting angiogenesis by VEGF

Elena Groppa^{1,2,‡,†}, Sime Brkic^{1,2,†}, Andrea Uccelli^{1,2}, Galina Wirth³, Petra Korpisalo-Pirinen³, Maria Filippova^{1,2}, Boris Dasen^{1,2}, Veronica Sacchi^{1,2,§}, Manuele Giuseppe Muraro^{1,2}, Marianna Trani^{1,2}, Silvia Reginato^{1,2}, Roberto Gianni-Barrera^{1,2}, Seppo Ylä-Herttuala^{3,4} & Andrea Banfi^{1,2,*} 

Abstract

Vascular endothelial growth factor (VEGF) is the master regulator of angiogenesis, whose best-understood mechanism is sprouting. However, therapeutic VEGF delivery to ischemic muscle induces angiogenesis by the alternative process of intussusception, or vascular splitting, whose molecular regulation is essentially unknown. Here, we identify ephrinB2/EphB4 signaling as a key regulator of intussusceptive angiogenesis and its outcome under therapeutically relevant conditions. EphB4 signaling fine-tunes the degree of endothelial proliferation induced by specific VEGF doses during the initial stage of circumferential enlargement of vessels, thereby limiting their size and subsequently enabling successful splitting into normal capillary networks. Mechanistically, EphB4 neither inhibits VEGF-R2 activation by VEGF nor its internalization, but it modulates VEGF-R2 downstream signaling through phospho-ERK1/2. *In vivo* inhibitor experiments show that ERK1/2 activity is required for EphB4 regulation of VEGF-induced intussusceptive angiogenesis. Lastly, after clinically relevant VEGF gene delivery with adenoviral vectors, pharmacological stimulation of EphB4 normalizes dysfunctional vascular growth in both normoxic and ischemic muscle. These results identify EphB4 as a druggable target to modulate the outcome of VEGF gene delivery and support further investigation of its therapeutic potential.

Keywords EphB4; EphrinB2; intussusception; vascular endothelial growth factor

Subject Categories Signal Transduction; Vascular Biology & Angiogenesis

DOI 10.15252/embr.201745054 | Received 23 August 2017 | Revised 3 March 2018 | Accepted 8 March 2018 | Published online 11 April 2018

EMBO Reports (2018) 19: e45054

Introduction

Angiogenesis plays a key role in the pathophysiology of a wide-spread variety of human diseases, both degenerative and neoplastic, as well as in physiological tissue regeneration [1]. Vascular endothelial growth factor-A (VEGF) is the master regulator of vascular growth in development and postnatal life, and it is therefore the key molecular target to promote the growth of new blood vessels in ischemic diseases, such as myocardial infarction, stroke, or peripheral vascular disease [2,3]. However, simple VEGF gene delivery for therapeutic angiogenesis has failed to prove clinical efficacy to date, despite the clear biological activity of the factor [2,4], highlighting the need to better understand the mechanisms of physiological vascular growth by VEGF, especially under therapeutically relevant conditions of factor delivery.

The best-understood mode of angiogenesis is sprouting, which is mostly studied during development, when specialized endothelial tip cells migrate from pre-existing vessels, followed by proliferating stalk cells, to invade surrounding avascular tissue [5]. However, blood vessels can also grow by the alternative mechanism of intussusception, or splitting angiogenesis, whereby rows of intraluminal endothelial pillars split pre-existing vessels longitudinally into new ones [6]. Intussusception is increasingly recognized as a therapeutically important mode of angiogenesis, both in tumor resistance to anti-angiogenic treatments and in reparative vascular growth [7–9], but very little is known about its molecular regulation due to a paucity of appropriate models.

Taking advantage of a cell-based platform that we developed for the controlled expression of specific and homogeneous doses of angiogenic factors *in vivo*, we previously found that (i) VEGF can induce either normal and functional capillary networks or aberrant angioma-like vascular structures depending on its concentration in the microenvironment around each producing cell *in vivo* [10] and (ii) VEGF doses required for therapeutic efficacy [11], induce robust vascular growth in skeletal muscle essentially through

1 Department of Biomedicine, University Hospital, University of Basel, Basel, Switzerland

2 Department of Surgery, University Hospital, Basel, Switzerland

3 A. I. Virtanen Institute, University of Eastern Finland, Kuopio, Finland

4 Heart Center, Kuopio University Hospital, Kuopio, Finland

*Corresponding author. Tel: +41 61 265 3507; Fax: +41 61 265 3990; E-mail: andrea.banfi@usb.ch

†These authors contributed equally to this work

‡Present address: The Biomedical Research Centre, The University of British Columbia, Vancouver, BC, Canada

§Present address: Genomics Institute of the Novartis Research Foundation, San Diego, CA, USA

intussusception [9]. Interestingly, both normal and aberrant vascular structures form through a first stage of circumferential enlargement within the first 4 days, followed by intussusceptive remodeling by 7 days [9], whereas the transition from normal to aberrant angiogenesis is determined by the retention or loss of pericytes during the initial stage of vascular enlargement [12].

Here, we took advantage of this unique and well-characterized model of VEGF dose-dependent intussusceptive angiogenesis to investigate its molecular regulation. We dissected the role of specific pericyte-mediated signaling pathways, and we identified a critical function for ephrinB2/EphB4 signaling, but not TGF- β or angiopoietin signaling. Specifically, we show that the endothelial receptor EphB4 controls the outcome of intussusceptive angiogenesis by fine-tuning the degree of endothelial proliferation caused by specific VEGF doses and therefore the size of initial vascular enlargement, without directly affecting VEGF-R2 activation, but rather modulating its downstream signaling through MAPK/ERK. Together, these results identify the ephrinB2/EphB4 pathway as a key regulator of intussusceptive angiogenesis and a druggable target to modulate the outcome of VEGF delivery.

Results

Generation and validation of blockers of pericyte-endothelium paracrine signaling

To determine whether and which pericyte-derived signals may control normal vascular morphogenesis induced by moderate VEGF doses, we blocked the three main signaling pathways responsible for the cross-talk between pericytes (P) and endothelial cells (EC), that is, the TGF- β 1, angiopoietin (Ang)/Tie2, and ephrinB2/EphB4 axes. A clonal myoblast population that homogeneously expresses moderate VEGF levels (V-low = 61 ± 2.9 ng/10⁶ cells/day) was selected to induce normal angiogenesis [9,13], or myoblasts that do not express VEGF as control (Ctrl). Both populations were transduced with retroviral vectors co-expressing soluble blockers of the TGF- β 1 (latency-associated peptide, LAP), Ang/Tie2 (sTie2Fc), and ephrinB2/EphB4 (sEphB4) signaling, together with a truncated version of CD4 (trCD4) in a bicistronic cassette (Fig EV1A) as a FACS-quantifiable surface marker [13] (Fig EV1B). ELISA measurements confirmed that all blocker-expressing V-low populations

maintained a similar VEGF production as the original V-low clone (V-low = 64 ± 3 , V-low LAP = 64 ± 6 , V-low sTie2Fc = 79 ± 4 , V-low sEphB4 = 62 ± 5 ng/10⁶ cells/day). Specific expression of each blocker was confirmed by RT-PCR on the *in vitro* cultured myoblast populations (Fig EV1C), while the functional activity of the secreted proteins was verified by appropriate *in vitro* assays on myoblast conditioned media (Fig EV1D–F).

Blockade of ephrinB2/EphB4 signaling, but not of TGF- β 1/TGF- β R or angiopoietin/Tie2, switches VEGF-induced angiogenesis from normal to aberrant

Simultaneous blockade of all three pathways of the P-EC cross-talk was achieved by co-implanting the individual blocker-expressing populations into hindlimb muscles of adult mice (Fig 1A). After 2 weeks, myoblasts expressing only the blockers in the absence of VEGF (Ctrl 3b) did not perturb the pre-existing vasculature compared to controls (Ctrl CD4). Low levels of VEGF induced the growth of normal mature capillaries, tightly associated with NG2⁺/ α -SMA⁻ pericytes, but co-expression of the three soluble inhibitors converted these into aberrant vascular structures, characterized by enlarged and irregular diameters, and covered by a patchy layer of SMA⁺ smooth muscle cells instead of pericytes (V-low 3b), similar to the angioma-like structures induced by another monoclonal myoblast population expressing high VEGF levels alone [10] (V-high = 137.7 ± 1.6 ng/10⁶ cells/day).

To determine whether any of the three signaling pathways was individually responsible for the switch, each blocker-secreting V-low population was injected separately (Fig 1B). By 2 weeks, ephrinB2/EphB4 blockade caused the appearance of irregularly enlarged aberrant vascular structures, similar to those induced by high VEGF alone, whereas neither TGF- β 1/TGF- β R nor Ang/Tie2 blockade affected the normal angiogenesis induced by V-low. Quantification of vessel diameter distributions showed that V-low induced angiogenesis characterized by homogeneous capillary-size vessels with a median of 4.0 μ m and 90th percentile of 6.1 μ m. However, inhibition of ephrinB2/EphB4 signaling gave rise to a fraction of significantly enlarged structures, with 13% of vessels having diameter > 10 μ m, compared to 2 and 1% that could be observed in muscles implanted with control cells expressing only sEphB4 and no VEGF, or with V-low cells alone, respectively (Fig 1C). The average size of vessels induced by V-low was also significantly increased

Figure 1. Blockade of ephrinB2/EphB4 signaling switches VEGF-induced angiogenesis from normal to aberrant.

- A, B Immunofluorescence staining of endothelium (CD31, red), pericytes (NG2, green), smooth muscle cells (α -SMA, cyan), and nuclei (DAPI, blue) on frozen sections of limb muscles injected with myoblast clones expressing different VEGF levels (V-low and V-high, respectively) or co-expressing low VEGF with blockers of the TGF- β 1, angiopoietin/Tie2, and ephrinB2/EphB4 pathways together (V-low 3b) or each individually (LAP, sTie2Fc, or sEphB4). Cells expressing only CD4 surface marker (Ctrl CD4) or blockers (Ctrl 3b) served as controls. Normal angiogenesis induced by V-low was switched to aberrant, enlarged, and smooth muscle-covered vessels, similar to those induced by high VEGF alone (V-high), in the presence of all three blockers or selectively by inhibition of ephrinB2/EphB4 signaling alone. Scale bar = 25 μ m.
- C, D Quantification of vessel diameters, displayed as distribution (C) or mean \pm SEM (D). A population of aberrantly enlarged vessels > 10 μ m is induced by ephrinB2/EphB4 blockade. $n = 3$ mice/group (Ctrl sEphB4 and V-low), $n = 5$ mice (V-low sEphB4); * $P < 0.05$ (Mann–Whitney test).
- E Immunofluorescence staining for mural cell markers (NG2 or α -SMA, both green) and basal lamina (laminin, purple) shows that aberrant vessels induced by ephrinB2/EphB4 blockade are associated with smooth muscle (α -SMA⁺ outside the basal lamina) rather than pericytes (NG2⁺ embedded inside the basal lamina). White arrows indicate an NG2⁺ pericyte (in V-low left panels) and an α -SMA⁺ smooth muscle cell (in the V-low sEphB4 right panels); *lumen of aberrant structure. Scale bar = 25 μ m.
- F Quantification of mural cell coverage of vessels induced by V-low or V-low sEphB4, shown as the ratio of NG2⁺/CD31⁺ and α -SMA⁺/CD31⁺ areas, or the ratio between the two markers (NG2/SMA). $n = 3$ mice (V-low), $n = 6$ mice (V-low sEphB4); * $P < 0.05$ (Mann–Whitney test).

by EphB4 blockade (V-low = $4.4 \pm 0.2 \mu\text{m}$ vs. V-low sEphB4 = $6.6 \pm 0.5 \mu\text{m}$, $P < 0.05$; Fig 1D). The nature of mural cells associated with vessels induced by V-low alone or with sEphB4 was

further investigated by co-staining for the vascular basal lamina. As can be seen in Fig 1E, normal capillaries induced by low VEGF were associated with NG2⁺ pericytes that were completely embedded in

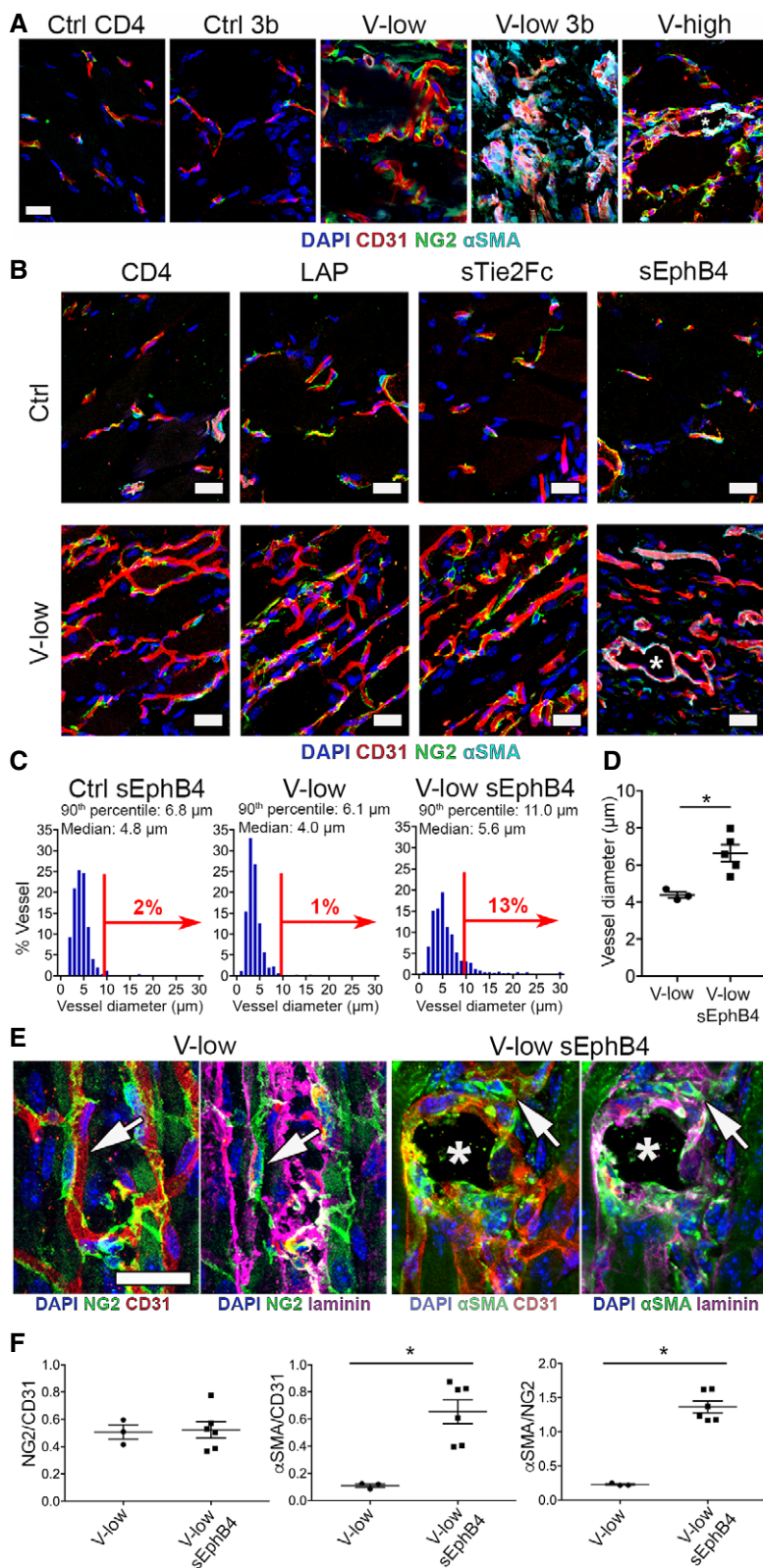


Figure 1.

the laminin-positive basal lamina, whereas the mural cells associated with the aberrant vascular structures induced in the presence of sEphB4 were both α -SMA⁺ and positioned externally to the basement membrane and were therefore identified as smooth muscle cells rather than pericytes. Quantification of NG2⁺ and α -SMA⁺ mural cell coverage (Fig 1F) showed that the transition from pericytes to smooth muscle cells by EphB4 blockade did not result in a loss of NG2, as both mural cell types retain expression of this marker. However, the α -SMA/CD31 ratio was significantly increased with sEphB4, as pericytes do not express α -SMA (V-low = 0.1 ± 0.0 vs. V-low sEphB4 = 0.7 ± 0.1 , $P < 0.05$), as well as the α -SMA/NG2 ratio (V-low = 0.2 ± 0.0 vs. V-low sEphB4 = 1.4 ± 0.1 , $P < 0.05$).

Intravascular staining by FITC-labeled tomato lectin, which binds to the luminal surface of endothelial structures only if they are connected to the systemic circulation, co-localized with endothelium staining (CD31), indicating that the aberrant structures caused by V-low sEphB4 cells were not simply endothelial clusters, but were functionally perfused (Fig EV2). This is in agreement with previous findings for angioma-like structures induced by high VEGF alone [11]. Further, staining for the apical- and basal-specific markers podocalyxin [14] and laminin confirmed that endothelium in both normal and aberrant vascular structures induced by V-low, V-low 3b, and V-low sEphB4 was functionally polarized into luminal and basal compartments (Appendix Fig S1). Lastly, to determine the evolution of the morphological changes caused by ephrinB2/EphB4 blockade, tissues were analyzed after 12 weeks, showing that the aberrant structures observed by 2 weeks continued growing in size (Appendix Fig S2).

Altogether, these results suggest that the ephrinB2/EphB4 pathway, but not TGF- β 1/TGF- β R and Ang/Tie2, has a function in the development of normal angiogenesis by low VEGF doses and its blockade causes the switch to an aberrant phenotype resembling the angioma-like vascular structures induced by high VEGF alone.

Activation of EphB4 signaling prevents aberrant angiogenesis induced by high VEGF doses

To complement the ephrinB2/EphB4 inhibition data above, we asked whether the pharmacological activation of EphB4 might prevent aberrant angiogenesis by high VEGF levels. A recombinant ephrinB2-Fc chimeric protein, whereby fusion with the immunoglobulin Fc portion enables the formation of dimers of ephrinB2 extracellular domains, was used to activate the EphB4 receptor [15]. V-high clonal myoblasts were injected in leg muscles of adult mice that were treated systemically with ephrinB2-Fc or Fc control protein by intraperitoneal injection [16]. Two weeks later, high VEGF induced heterogeneous enlarged vascular structures associated with smooth muscle cells (Fig 2A). As normal muscle capillaries have homogeneous sizes smaller than 10 μ m, vessel diameter distribution was quantified and showed that 26% of induced structures were larger than 10 μ m (Fig 2B). On the other hand, treatment with ephrinB2-Fc yielded networks of pericyte-covered normal capillaries (Fig 2A), similar to those induced by V-low alone (Fig 1B) and with a homogeneous diameter distribution (Fig 2B; median = 5.1 μ m and 6% of vessels larger than 10 μ m). The average vessel size was also significantly reduced by ephrinB2-Fc treatment (V-high + Fc = $9.5 \pm 0.3 \mu$ m vs. V-high +

ephrinB2-Fc = $5.8 \pm 0.2 \mu$ m, $P < 0.05$; Fig 2C). Again, podocalyxin and laminin staining confirmed proper apico-basal polarization of the endothelial structures (Appendix Fig S1).

These results were confirmed independently of cell-based VEGF delivery, using an optimized fibrin-based platform that we recently developed for controlled release of VEGF recombinant protein at specific doses and with duration up to 4 weeks in skeletal muscle [17]. An engineered version of murine VEGF₁₆₄ was fused to the transglutaminase substrate octapeptide NQEQVSP (V- α_2 -PI₁₋₈-VEGF), to allow its covalent cross-linking into fibrin hydrogels by the coagulation factor XIIIa and release only by enzymatic cleavage [18,19]. Fibrin hydrogels containing a high dose of α_2 -PI₁₋₈-VEGF (50 μ g/ml), which we previously found to induce aberrant angiogenesis [17], were injected in gastrocnemius muscles and the animals were treated systemically with ephrinB2-Fc. In agreement with the myoblast-based experiments, ephrinB2-Fc treatment prevented the appearance of heterogeneous, enlarged, and smooth muscle-covered vascular structures induced by the high VEGF dose, yielding instead networks of pericyte-covered capillaries by 7 days (Fig 2D), with a more homogeneous size distribution (Fig 2E) and significantly smaller diameters (fibrin-High V + Fc = $10.0 \pm 0.6 \mu$ m vs. fibrin-High V+ephrinB2-Fc = $6.9 \pm 0.5 \mu$ m, $P < 0.05$; Fig 2F).

The observed prevention of aberrant vascular structures could be due to either their switch to a normal phenotype or to their regression. Since regressing vessels leave behind their basal lamina, a staining for laminin was performed to detect so-called empty sleeves of vascular basement membrane, which provide a sort of historical record of pre-existing vessels [20]. As shown in Fig EV3, by 7 days after injection of V-high myoblasts we could not identify laminin sleeves in the tissues treated with ephrinB2-Fc compared with the controls treated with Fc only. On the other hand, many empty sleeves were clearly visible in positive control tissues treated with the potent VEGF blocker aflibercept, which caused the regression of vascular structures induced by high VEGF, suggesting that EphB4 stimulation could prevent the formation of aberrant structures by regulating VEGF-induced vascular morphogenesis.

Altogether, the results of these inhibition and stimulation experiments indicate that the ephrinB2/EphB4 signaling pathway determines whether a specific VEGF dose induces normal or aberrant angiogenesis.

EphrinB2/EphB4 signaling controls the degree of initial vascular enlargement induced by VEGF

In order to understand how ephrinB2/EphB4 signaling regulates the switch between normal and aberrant angiogenesis, we investigated the effects of EphB4 inhibition or stimulation on the early morphogenic events after delivery of low and high VEGF levels, respectively, which comprise an initial stage of circumferential enlargement of pre-existing vessels by 3–4 days, followed by longitudinal splitting by 7 days [9]. As shown in Fig 3A and B, by 4 days both V-low and V-high myoblasts induced vascular enlargements, whose diameter was proportional to VEGF dose (V-low: median = 8.8 μ m, average = $10.5 \pm 0.8 \mu$ m; V-high: median = 11.9 μ m, average = $14.5 \pm 1.7 \mu$ m). However, co-expression of sEphB4 increased the average size of vascular enlargements induced by low VEGF (V-low sEphB4 = $15.1 \pm 1.1 \mu$ m, $P < 0.01$ vs. V-low; Fig 3E) to values similar to those caused by high VEGF alone (Fig 3F). Conversely, EphB4

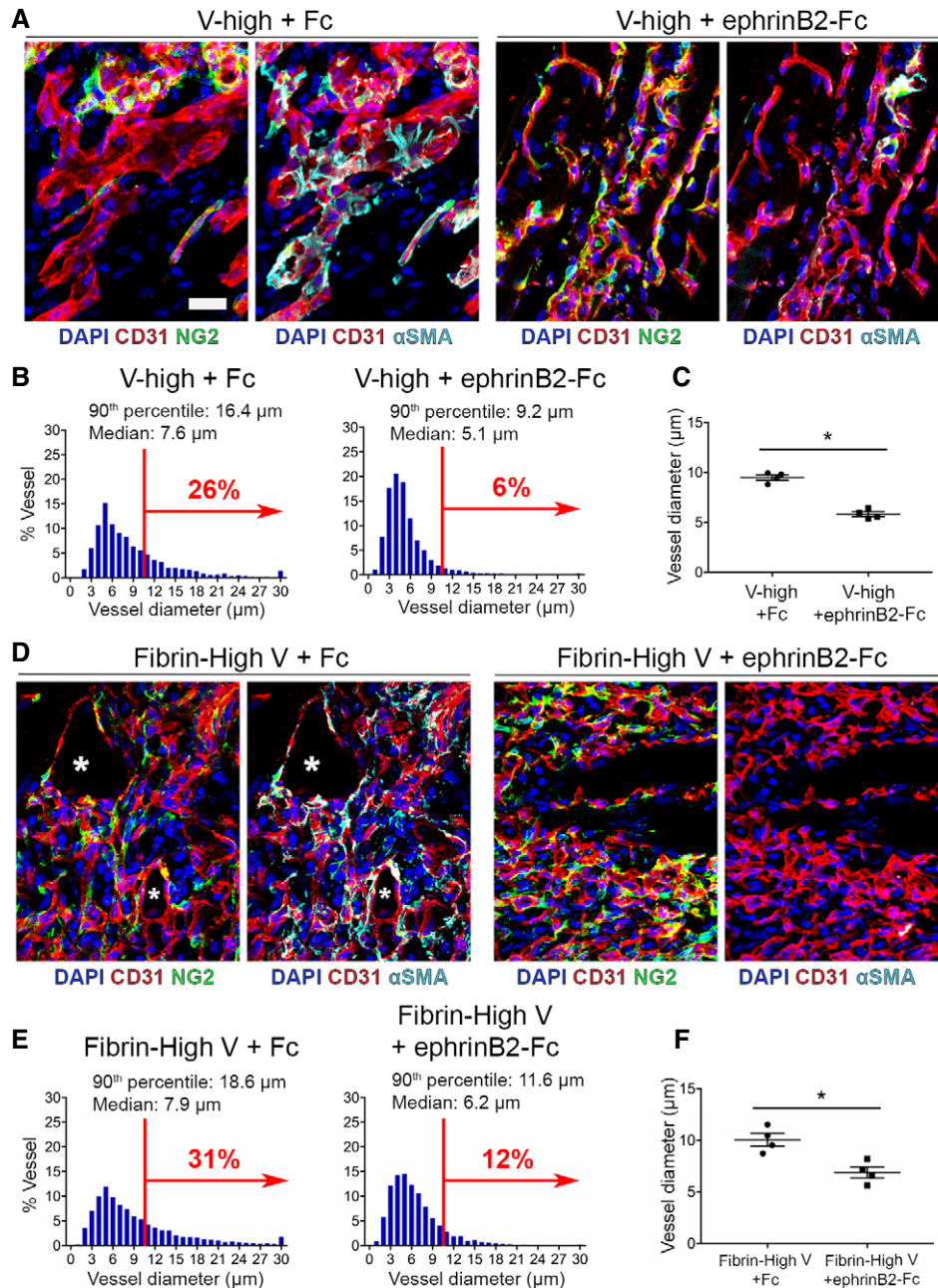


Figure 2. Activation of EphB4 by ephrinB2-Fc prevents aberrant angiogenesis.

A–F A high VEGF dose was delivered to limb muscles of mice either by genetically modified myoblasts (V-high, A–C) or as fibrin-bound recombinant protein (fibrin-High V, D–F), and animals were treated intraperitoneally with ephrinB2-Fc or control Fc recombinant protein. Immunostaining (A, D) of frozen sections for endothelium (CD31, red), pericytes (NG2, green), smooth muscle cells (α -SMA, cyan), and nuclei (DAPI, blue) showed that, with both delivery platforms, ephrinB2-Fc treatment prevented the induction of aberrant vascular structure by high VEGF and yielded only normal capillary networks. *lumens of aberrant structures in (D); scale bar = 25 μ m. Quantification (B, C, E, and F) of vessel diameters showed a consistent and significant decrease in vessel sizes after treatment with ephrinB2-Fc. Results are shown as diameter distributions (B, E) and mean \pm SEM (C, F). Red arrows and numbers indicate the fraction of vessel diameters > 10 μ m. $n = 4$ mice; * $P < 0.05$ (Mann–Whitney test).

stimulation by systemic treatment with ephrinB2-Fc significantly reduced the diameter of vascular enlargements induced by high VEGF (Fig 3F; V-high + ephrinB2-Fc = 9.5 ± 1.0 μ m, $P < 0.05$ vs. V-high + Fc). By 7 days, the smaller enlargements induced by V-low remodeled to normal capillaries, whereas the larger ones induced by

V-high failed to split and some segments gave rise to aberrantly enlarged structures (Fig 3C and D). However, upon modulation of EphB4 signaling, the fate of initial enlargements was determined by their size rather than the dose of VEGF. In fact, ephrinB2-Fc treatment caused proper remodeling to homogeneous normal capillary

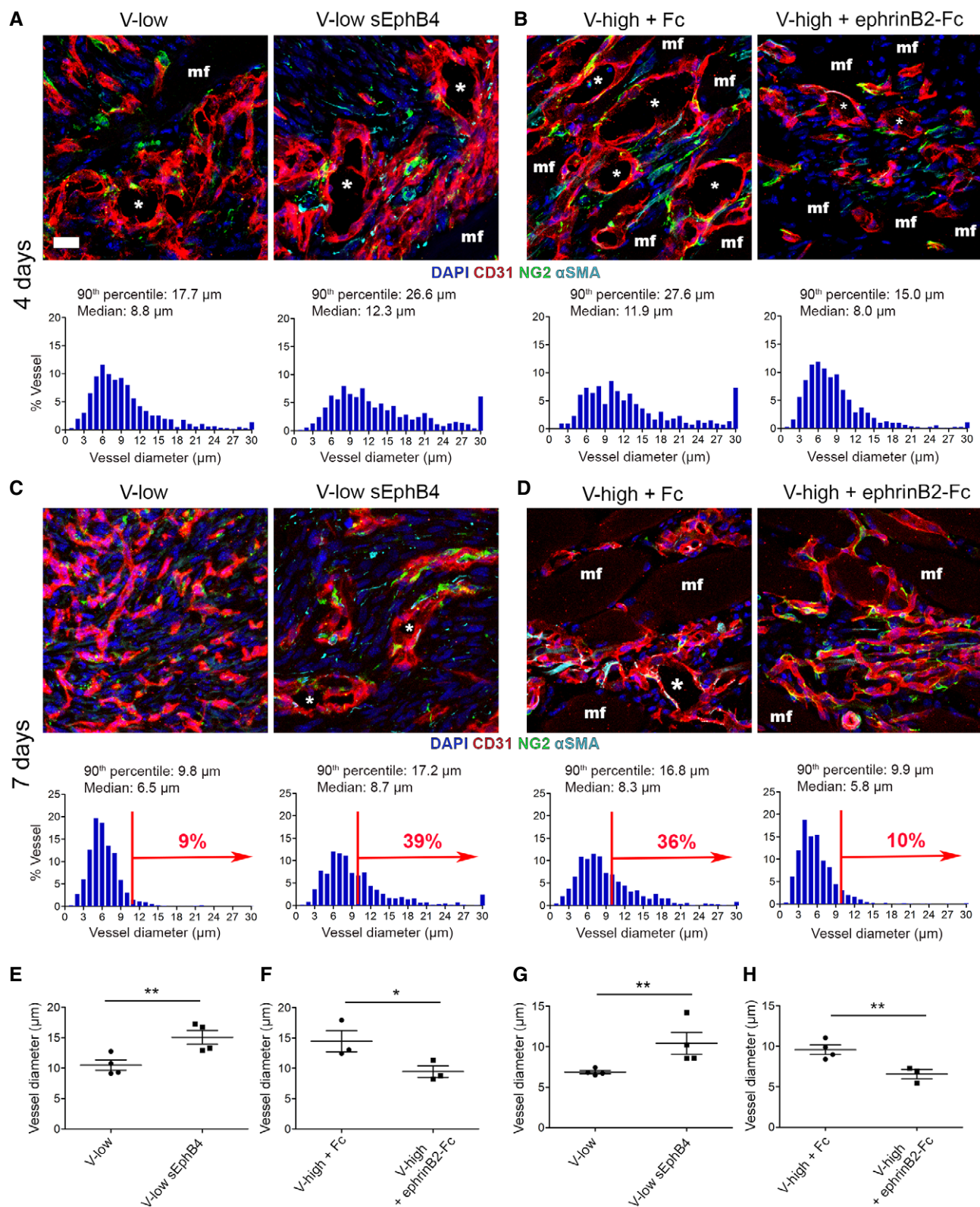


Figure 3.

networks despite high VEGF, whereas EphB4 inhibition led to failure of splitting despite low VEGF (Fig 3C and D), as shown also by the quantification of vessel diameters (Fig 3G and H).

The transition from normal to aberrant angiogenesis by increasing VEGF doses has been shown to be associated with loss of pericytes at the initial stage of circumferential enlargement 4 days after

Figure 3. EphrinB2/EphB4 signaling regulates the degree of vascular enlargement by VEGF dose.

Mouse limb muscles were implanted with myoblast clones expressing low (V-low) or high (V-high) VEGF doses, while the ephrinB2/EphB4 signaling pathway was inhibited by co-expression of the sEphB4 blocker (V-low sEphB4) or stimulated by intraperitoneal treatment with ephrinB2-Fc or control Fc protein.

- A–D Immunostaining of frozen sections (upper panels) stained for endothelium (CD31, red), pericytes (NG2, green), smooth muscle cells (α -SMA, cyan), and nuclei (DAPI, blue) and quantification of vessel diameter distribution (lower panels) showed that 4 days after VEGF delivery, the size of initial circumferential enlargements was increased by ephrinB2/EphB4 inhibition and reduced by its stimulation (A, B). By 7 days, after completion of remodeling, EphB4 inhibition switched normal angiogenesis by V-low to aberrant (C) and its stimulation converted aberrant structures by V-high into normal capillary networks (D). Red arrows and numbers indicate the fraction of vessel diameters $> 10 \mu\text{m}$. *lumen of aberrant structures; mf, muscle fibers; scale bar, $25 \mu\text{m}$.
- E–H Quantification of vessel diameters after 4 days (E, F) and 7 days (G, H). Values represent means of individual measurements in each sample \pm SEM. $n = 3$ –4 independent samples/group; * $P < 0.05$ and ** $P < 0.01$ (one-tailed t -test, after data normalization by logarithmic-transformation).

factor delivery [9]. Analysis of mural cell coverage showed that inhibition of ephrinB2/EphB4 signaling did not interfere with pericyte coverage of initial vascular enlargements induced by low VEGF, both at 3 and at 4 days (Fig 4A). In the presence of low VEGF alone, pericytes were positive for NG2 and negative for α -SMA, as expected and typical for microvasculature of skeletal muscle. However, upon co-expression of the sEphB4 blocker, most mural cells associated with vascular enlargements became double-positive for both NG2 and α -SMA (Fig 4A). Co-staining for laminin revealed that NG2⁺/ α -SMA⁺ mural cells were completely embedded into the vascular basement membrane (Fig 4B), thereby confirming their identity as pericytes and excluding a transition to a smooth muscle cell phenotype at this stage [21]. In line with this, gene expression analysis in muscles 3 days after myoblast implantation showed that both *Pdgfb* and its receptor *Pdgfrb*, which regulate pericyte recruitment, were similarly upregulated after stimulation with VEGF regardless of EphB4 inhibition (Fig 4C).

Altogether, these results indicate that ephrinB2/EphB4 signaling (i) modulates the degree of vascular enlargement induced by a given VEGF dose, determining whether splitting into normal capillaries succeeds or fails; and (ii) does not interfere with pericyte recruitment.

EphrinB2/EphB4 signaling modulates VEGF-induced endothelial proliferation

The initial vascular enlargement caused by VEGF overexpression is associated with endothelial proliferation [9]. Therefore, we investigated whether ephrinB2/EphB4 signaling may regulate the amount of endothelial proliferation induced by specific VEGF doses *in vivo*. The degree of proliferation depends both on the proportion of cycling cells and on the speed with which they cycle. Therefore, we performed co-immunostaining for CD31 and either Ki67, which is expressed throughout all phases of the cell cycle and marks all proliferating cells, but not quiescent ones in G0 [22], or phosphorylated histone H3 (pHH3), which is only detectable during the G2-M

phase [23,24]. Since the duration of the cell cycle depends on how long cells spend in G1, while the G2-M phase has a constant duration, the proportion of pHH3⁺ cells reflects how often proliferating cells are cycling and provides an indication of the endothelial proliferation rate.

Vascular enlargements induced by V-low alone or with sEphB4 co-expression contained similar proportions of Ki67⁺ endothelial cells at both 3 and 4 days after myoblast implantation (Fig 5A). However, at 3 days, EphB4 inhibition caused a significant increase by about 40% in the frequency of pHH3⁺ endothelial cells compared to low VEGF alone (Fig 5B), suggesting a faster proliferation rate. At 7 days, most of the endothelial cells in the normal capillary networks induced by low VEGF were Ki67[−] and became quiescent, as expected, whereas 40% of the endothelium in the aberrant vascular structures generated in the presence of EphB4 blockade were still proliferating (Fig 5A), similarly to those induced by high VEGF alone (Fig 5C). Conversely, EphB4 stimulation by systemic ephrinB2-Fc treatment caused a significant reduction in the proportion of Ki67⁺ endothelial cells at both 4 and 7 days (Fig 5C), while the frequency of pHH3⁺ endothelial cells was significantly reduced by about 40% already by 3 days (Fig 5D), reducing it to a similar value as that induced by low VEGF alone (Fig 5B). Furthermore, EphB4 expression in angiogenic vessels *in vivo* was restricted to the endothelium, with no detectable signal on associated pericytes, and was not modified by either VEGF dose or its own stimulation by ephrinB2-Fc or inhibition by sEphB4 (Fig EV4).

To determine whether EphB4 signaling regulated endothelial proliferation directly or indirectly, we investigated the effects of ephrinB2-Fc treatment on endothelial cell cycle progression *in vitro*. Human dermal microvascular cells (HDMEC), which strongly express EphB4 and are mostly negative for ephrinB2 (Appendix Fig S3), were stimulated with recombinant VEGF or with the unrelated strong mitogen FGF-2 [25], with or without treatment with recombinant ephrinB2-Fc, and cell cycle analysis was performed by FACS after staining for Ki67 and pHH3 (Fig 5E). As shown in Fig 5F, in control conditions (no VEGF and 2,000 ng/ml of ephrinB2-Fc), about

Figure 4. Inhibition of ephrinB2/EphB4 signaling does not prevent pericyte recruitment.

Muscles were harvested 3 and 4 days after implantation of V-low or V-low sEphB4 myoblast clones.

- A Immunofluorescence staining of endothelium (CD31, red), pericytes (NG2, green), smooth muscle cells (α -SMA, cyan), and nuclei (DAPI, blue). In both conditions, initial vascular enlargements after 3 and 4 days were tightly associated with mural cells displaying a pericyte morphology, which, however, upregulated α -SMA expression in the presence of EphB4 blockade. *lumen of vascular enlargements; scale bar = $25 \mu\text{m}$.
- B Co-staining for laminin (LAM, red) confirmed the pericyte identity of both α -SMA-positive and α -SMA-negative mural cells, as both were embedded inside the endothelial basal lamina. *lumen of vascular enlargements; scale bar = $25 \mu\text{m}$.
- C Gene expression of *Pdgfb* and *Pdgfrb* was quantified in skeletal muscles 3 days after myoblast implantation and expressed as fold-change vs. control muscles. Mean \pm SEM; $n = 4$ independent samples/group; *** $P < 0.001$, **** $P < 0.001$ vs. Ctrl (*) or vs. sEphB4 (#) (one-way ANOVA with Bonferroni multiple comparisons test, after data normalization by logarithmic-transformation).

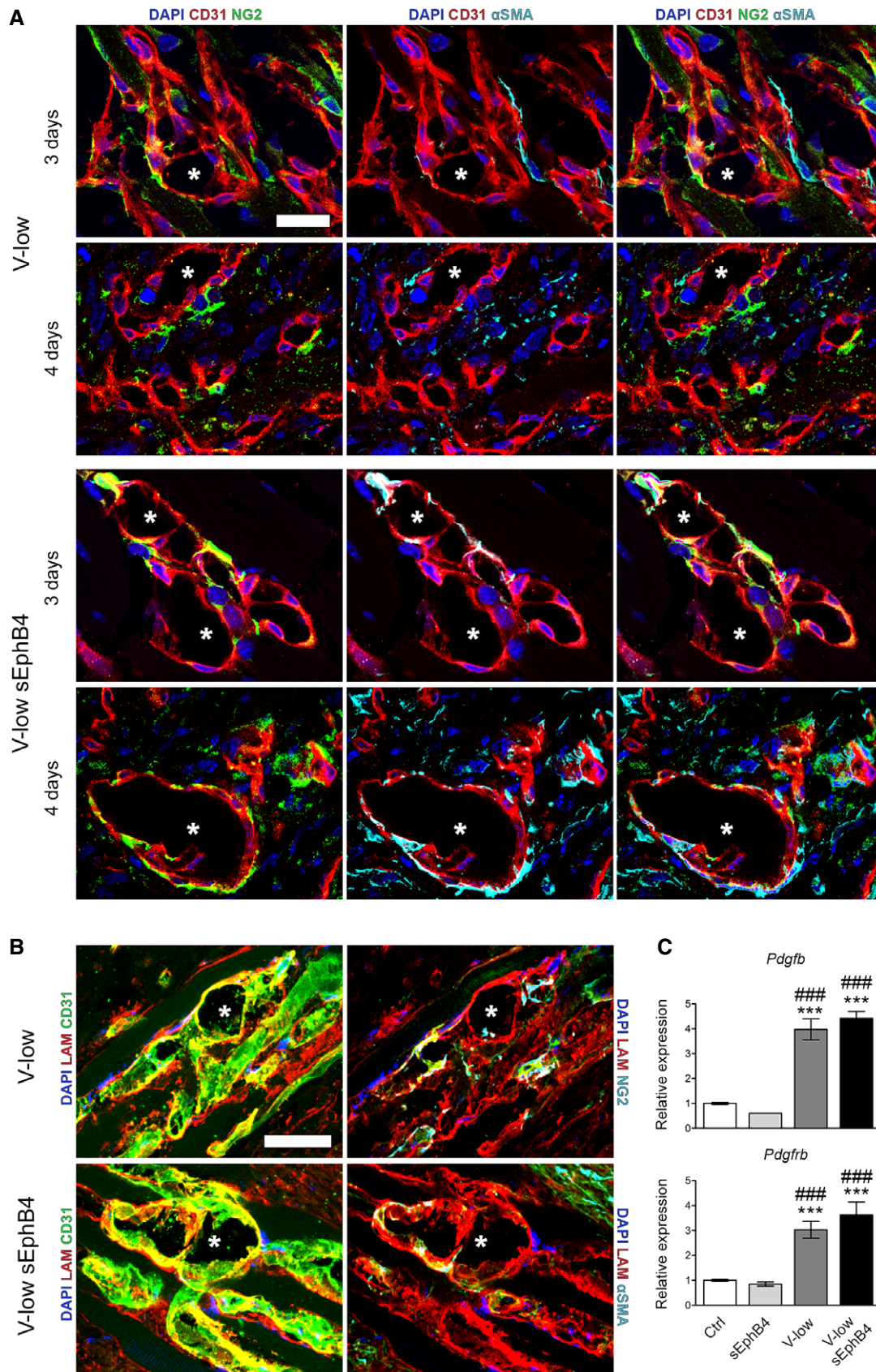


Figure 4.

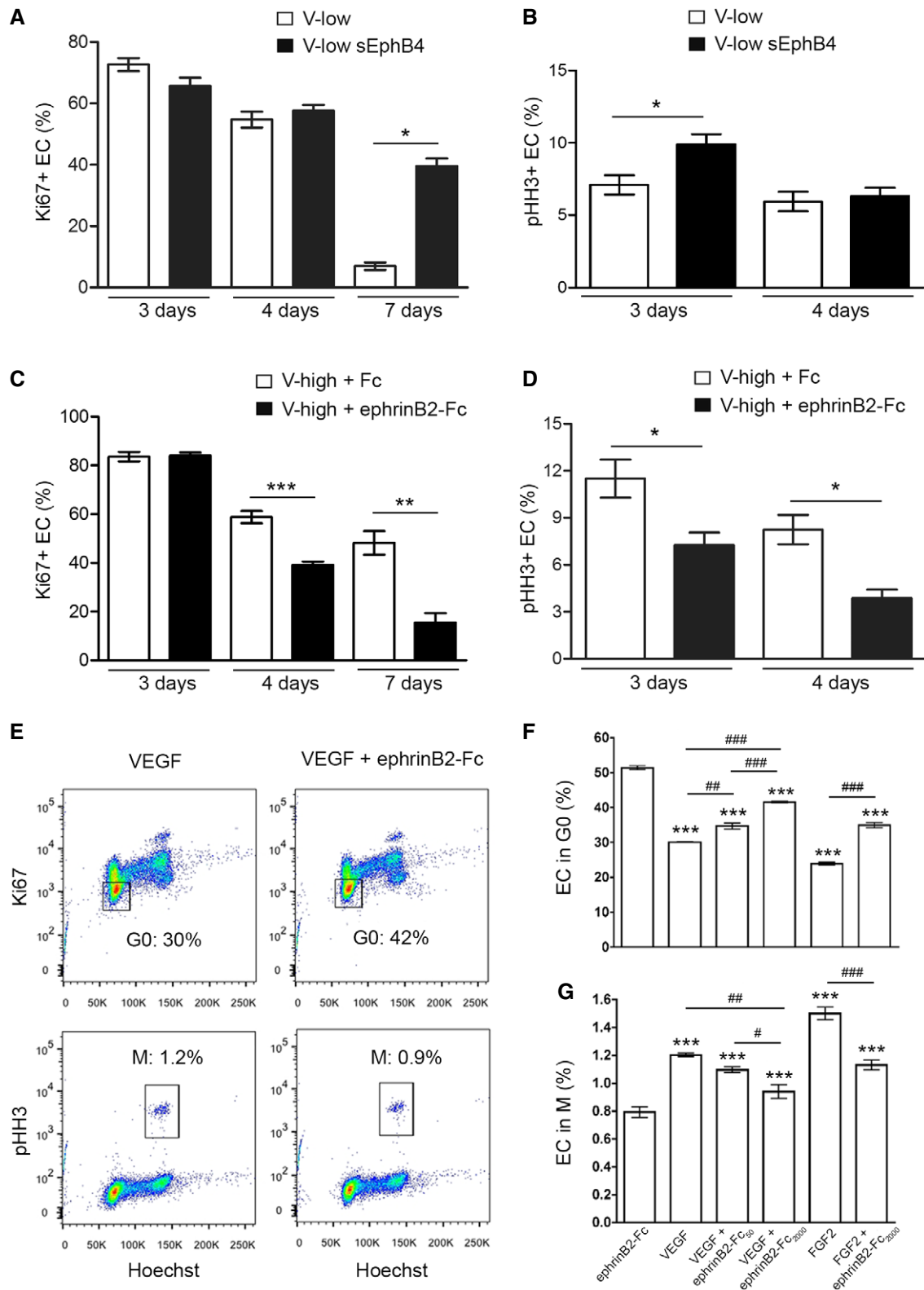


Figure 5.

50% of HDMEC were in G0. VEGF stimulation reduced this percentage to 30%, but treatment with ephrinB2-Fc (50 and 2,000 ng/ml) significantly and dose-dependently increased the proportion of non-

cycling cells to 40%. Conversely, VEGF stimulation increased the amount of cells undergoing mitosis in the G2-M phase by about 50% (from 0.8 to 1.2%), while ephrinB2-Fc treatment dose-dependently

Figure 5. EphrinB2/EphB4 signaling modulates endothelial proliferation.

A–D Muscles were harvested 3, 4, and 7 days after implantation of V-low or V-low sEphB4 clones, or V-high cells while treating animals systemically with ephrinB2-Fc or control Fc proteins. Endothelial proliferation was assessed by quantifying the percentage of endothelial cells positive for Ki67, which marks all cycling cells (A and C), or phosphorylated histone H3, which marks only cells in the G2/M phase (pHH3, B, and D), by immunofluorescence staining on frozen muscle sections. EphB4 inhibition specifically increased the rate of endothelial proliferation (pHH3⁺ cells) and its stimulation by ephrinB2-Fc conversely decreased it. Mean ± SEM; *n* = 4 independent samples/group; **P* < 0.05, ***P* < 0.01, and ****P* < 0.001 (one-way ANOVA with Bonferroni multiple comparisons test).

E–G Human dermal microvascular endothelial cells (HDMEC) were treated *in vitro* with recombinant VEGF or FGF2, while EphB4 was stimulated with ephrinB2-Fc (50 or 2,000 ng/ml). Cell cycle analysis was performed by FACS after staining for Ki67 and pHH3 (E), and the proportion of cells withdrawn from cycle (G0) or in mitosis (M) were quantified (F, G). EphB4 stimulation dose-dependently increased quiescence and decreased mitosis by both mitogens. Mean ± SEM; *n* = 3 independent samples/group; ****P* < 0.001 vs. ephrinB2-Fc control, #*P* < 0.05, ###*P* < 0.01 and ####*P* < 0.001 (one-way ANOVA with Bonferroni multiple comparisons test).

reversed this effect (Fig 5G). Notably, the anti-proliferative effect of ephrinB2-Fc treatment was not restricted to VEGF, as it similarly reduced the mitogenic effects of FGF-2 (Fig 5F and G).

FGF2 upregulation has been associated with intussusceptive angiogenesis during avian kidney development [26]. Therefore, we investigated expression levels of *Fgf2* and *Vegfa* 3 days after implantation of V-low cells alone or with EphB4 blockade. *Fgf2* was upregulated during VEGF-induced angiogenesis, but it was not further increased by EphB4 inhibition (Fig EV5A). Also, total *Vegfa* was significantly increased in tissues implanted with V-low-expressing myoblasts, but without differences in the presence of sEphB4 (Fig EV5B), whereas endogenous *Vegfa* was not upregulated in any condition (Fig EV5C). Further, the degree of upregulation of endogenous *Fgf2* was threefold to sixfold lower than the increase in total *Vegfa* caused by V-low myoblast implantation (Fig EV5D). Therefore, the switch from normal to aberrant angiogenesis caused by EphB4 inhibition did not depend on changes in either VEGF or FGF2 expression.

Thus, combined *in vivo* and *in vitro* analyses indicate that EphB4 signaling regulates endothelial proliferation by modulating the mitogenic activity of VEGF.

EphB4 modulates VEGF signaling output downstream of VEGF-R2 activation

In order to determine the mechanism by which EphB4 modulates VEGF activity, we assessed whether EphB4 stimulation regulated VEGF-R2 internalization, phosphorylation, or downstream signaling in HDMEC *in vitro* [27,28]. VEGFR-2 internalization after treatment with VEGF was analyzed by FACS (Fig 6A). VEGF stimulation strongly reduced the staining for surface VEGF-R2 without changing the total amount of VEGF-R2 expressed by the cells. While surface receptor staining could be restored by co-treatment with the VEGF-R2 receptor tyrosine kinase inhibitor axitinib [29], this was not

observed upon co-treatment with 2,000 ng/ml of ephrinB2-Fc. Quantification of the fraction of VEGF-R2 internalization (Fig 6B) confirmed that axitinib could robustly prevent VEGF-induced VEGF-R2 internalization, while ephrinB2-Fc caused a very small, albeit significant, reduction by < 5%. Neither axitinib nor ephrinB2-Fc had any effect in the absence of VEGF stimulation. These results were confirmed by an enzymatic cleavage protection assay and Western blot analysis (Appendix Fig S4), showing that ephrinB2-Fc treatment did not reduce the amount of VEGF-R2 that was internalized, and therefore protected from proteolytic degradation, upon VEGF stimulation.

Phosphorylation of VEGF-R2 was quantified after staining with a specific antibody for phosphotyrosine 1175 (pTyr1175), which is the key residue by which VEGF-R2 activates the MAPK/ERK pathway and stimulates cell proliferation [30]. EphrinB2-Fc treatment did not reduce the increase in pTyr1175 caused by VEGF (Fig 6C), suggesting that EphB4 stimulation did not directly affect VEGF-R2 activation. The effect of EphB4 activation on VEGF signaling downstream of the receptor was investigated by quantifying the expression of the VEGF-R2 target genes *Esm-1/Endocan* and *Igfbp3*. As shown in Fig 6D, both genes were upregulated by VEGF in HDMEC *in vitro*, as expected. However, ephrinB2-Fc treatment did not affect the expression of *Esm-1/Endocan*, which is regulated by the PI3-kinase/Akt signal transduction pathway [31], but it significantly down-regulated expression of *Igfbp3*, which is instead also regulated by ERK1/2 signaling [32,33]. Therefore, the effects of EphB4 signaling on VEGF-induced ERK1/2 activation were assessed *in vivo* by quantifying the percentage of endothelial cells positive for phosphorylated ERK1/2 (pERK1/2) in the initial vascular enlargements induced 3 and 4 days after implantation of myoblasts expressing low or high VEGF levels and in the presence of EphB4 inhibition or stimulation, respectively, similarly to the experimental setup described in Fig 3. After 3 days, about 10% of endothelial cells in

Figure 6. EphB4 regulates VEGF-induced phosphorylation of endothelial ERK1/2 downstream of VEGF-R2 activation.

HDMEC were treated *in vitro* with VEGF alone or together with ephrinB2-Fc or the VEGF-R2 small molecule inhibitor axitinib as a positive control.

A, B VEGF-R2 internalization was quantified by FACS. Mean ± SEM; *n* = 6 independent samples/group; ***P* < 0.01 and ****P* < 0.001 vs. not stimulated control, #*P* < 0.05, ###*P* < 0.001 (one-way ANOVA with Bonferroni multiple comparisons test).

C VEGF-R2 phosphorylation at tyrosine Y1175 (C) was quantified by immunocytochemistry. Mean ± SEM; *n* = 4 independent samples/group; **P* < 0.05 and ***P* < 0.01 vs. not stimulated control (one-way ANOVA with Bonferroni multiple comparisons test).

D Expression of VEGF-R2 target genes *Igfbp3* and *Esm1* was quantified by real-time qRT-PCR. Mean ± SEM; *n* = 8 independent samples/group; **P* < 0.05, ***P* < 0.01, and ****P* < 0.001 vs. not stimulated control, ####*P* < 0.001 (one-way ANOVA with Bonferroni multiple comparisons test, after data normalization by logarithmic-transformation).

E–H Muscles were harvested 3 and 4 days after implantation of V-low or V-low sEphB4 clones, or V-high cells while treating animals systemically with ephrinB2-Fc or control Fc proteins. Frozen sections were immunostained for phosphorylated ERK1/2 (p-ERK1/2) and the endothelial junctional protein VE-cadherin (VE-CAD) (E, G), and the percentage of p-ERK1/2-positive endothelial cells was quantified (F, H). EphB4 inhibition and stimulation, respectively, increased and decreased ERK1/2 activation downstream of VEGF-R2. *in IF panels = lumens of vascular enlargements. Scale bar = 20 μm. Mean ± SEM; *n* = 4 independent samples/group; **P* < 0.05 and ****P* < 0.001 (one-way ANOVA with Bonferroni multiple comparisons test).

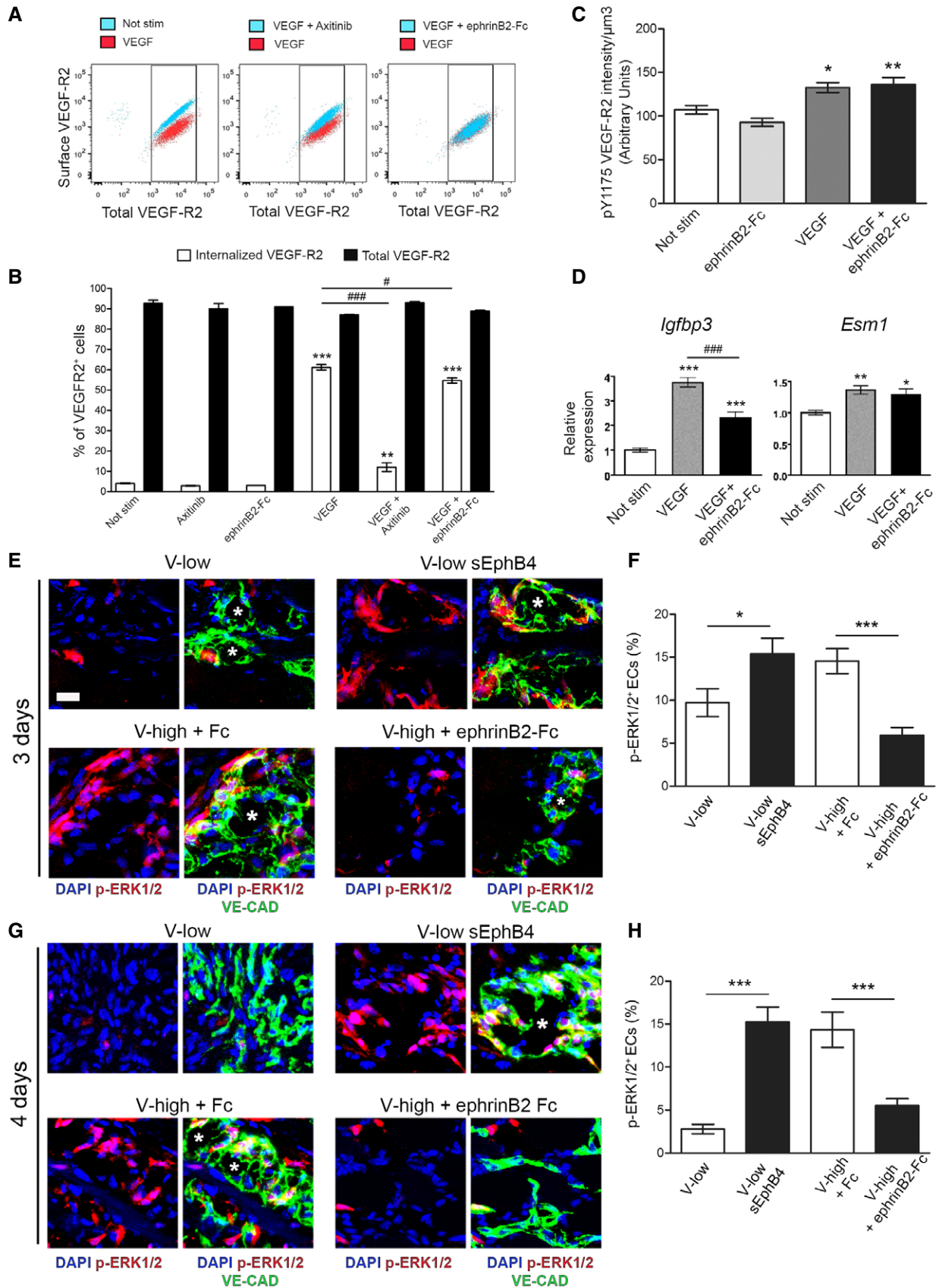


Figure 6.

vascular enlargements induced by low VEGF stained positive for pERK1/2, but EphB4 inhibition increased this proportion to about 15%, which was similar to that induced by high VEGF alone. Conversely, EphB4 activation by treatment with ephrinB2-Fc significantly reduced the amount of pERK1/2-positive endothelial cells in structures induced by high VEGF to levels similar to those of low VEGF alone (Fig 6E and F). By 4 days, pERK1/2-positive cells dropped to about 3% with low VEGF alone, but EphB4 inhibition caused this fraction to remain at about 15%, similarly to high VEGF alone, and EphB4 activation in the presence of high VEGF again reduced it significantly to about 5% (Fig 6G and H), in agreement with the day 3 results.

Altogether, these *in vitro* and *in vivo* data show that EphB4 activation by ephrinB2 modulates endothelial proliferation induced by specific VEGF doses without affecting VEGF-R2 activation, but rather by modulating the degree of ERK1/2 activation downstream of the receptor.

EphB4 prevents aberrant angiogenesis by VEGF through ERK1/2

Based on these results, we sought to investigate whether ERK1/2 activity is required for EphB4 function in regulating VEGF-induced intussusceptive angiogenesis. Therefore, we asked whether ERK1/2 inhibition could reverse the switch from normal to aberrant vascular growth caused by EphB4 blockade. After implantation with V-low and V-low sEphB4 myoblasts, animals were treated with three different doses (3, 6, and 12.5 mg/kg) of the potent and selective ERK1/2 inhibitor SCH772984 [34] or vehicle. The higher dose of 12.5 mg/kg proved toxic to the animals and therefore was not evaluated further. As shown in Fig 7A and B, after 4 days 5.0 ± 1.0% of endothelial cells in vascular enlargements induced by V-low stained positive for pERK1/2 and this was increased to 15.7 ± 0.9% by sEphB4 ($P < 0.001$), in agreement with the results in Fig 6H. Treatment with 6 mg/kg SCH772984 prevented this increase (7.5 ± 0.4%, $P < 0.01$ vs. V-low sEphB4), whereas 3 mg/kg was ineffective (12.9 ± 1.9%, $P = \text{n.s.}$ vs. V-low sEphB4). Quantification of vessel diameters at the 4-day time-point (Fig 7C and D) showed that, in agreement with the effects on pERK1/2 activity, the increase in vessel size caused by sEphB4 (diameter: V-low = 9.7 ± 0.2 μm vs. V-low sEphB4 = 14.1 ± 0.8 μm, $P < 0.01$) was prevented by 6 mg/kg SCH772984 (9.2 ± 0.2 μm, $P < 0.001$ vs. V-low sEphB4), but not by 3 mg/kg (12.9 ± 0.9 μm, $P = \text{n.s.}$ vs. V-low sEphB4).

Based on these results, we investigated the effects of ERK inhibition on the evolution of angiogenesis induced by V-low and V-low sEphB4 cells. Animals were treated systemically with

6 mg/kg of SCH772984 or vehicle for 7 days, as during this time intussusceptive remodeling is completed, and vascular morphology and quantity were evaluated after 2 weeks. The smooth muscle-covered aberrant structures induced by EphB4 blockade were prevented by ERK inhibition, yielding instead a normal capillary network similar to that generated by low VEGF alone (Fig 7E). Quantification of vessel diameters (Fig 7F) confirmed that sEphB4 caused the appearance of significantly enlarged vascular structures compared to V-low (V-low = 4.7 ± 0.1 μm vs. V-low sEphB4 = 7.1 ± 0.4 μm, $P < 0.01$), but this was prevented by ERK inhibition (5.5 ± 0.3 μm, $P < 0.05$ vs. V-low sEphB4). However, normal angiogenesis was not impaired, as vessel length density was similarly increased about threefold in all groups compared to controls, regardless of ERK inhibition (Fig 7G). Therefore, these data show that induction of aberrant angiogenesis by EphB4 blockade requires ERK1/2 activity.

EphB4 stimulation prevents aberrant angiogenesis by uncontrolled adenoviral VEGF gene delivery both in normal and in ischemic muscle

We sought to extend our findings, obtained with a controlled myoblast-based gene delivery platform, to a gene delivery system appropriate for clinical translation as a gene therapy approach. Therefore, first we tested whether ephrinB2-Fc treatment could prevent aberrant angiogenesis induced by intramuscular delivery of a VEGF-expressing adenoviral vector (Ad-mVEGF) in immune-deficient SCID mice, to avoid the confounding factor of immune clearance of the viral vector [35]. After 2 weeks, Ad-mVEGF induced several enlarged and multi-lumenized, smooth muscle-covered aberrant vascular structures, but ephrinB2-Fc treatment prevented their appearance and yielded only normal capillary networks associated with NG2⁺ pericytes (Fig 8A), with more homogeneous diameters (Fig 8B) and smaller in size (Fig 8C; Ad-mVEGF + Fc = 7.4 ± 0.5 μm vs. Ad-mVEGF + ephrinB2-Fc = 6.1 ± 0.2 μm, $P < 0.05$).

Lastly, we investigated whether this approach could ensure normal and functional angiogenesis also during ischemia, in conditions where a variety of endogenous angiogenic pathways are upregulated and tissue repair is occurring. Acute hindlimb ischemia was induced in immune-competent hyperlipidemic mice [36]. Intramuscular adenoviral transfer of the human VEGF₁₆₅ gene (Ad-hVEGF) induced capillary growth compared to control vector (Ad-LacZ), but also formation of aberrant, lacunae-like vascular structures (Fig 8D). Concomitant systemic treatment with ephrinB2-Fc prevented the formation of highly enlarged vascular lacunae

Figure 7. Aberrant angiogenesis by EphB4 blockade requires ERK1/2 activity *in vivo*.

- A–D Muscles were harvested 4 days after implantation of V-low or V-low sEphB4 clones, while treating animals systemically with the selective ERK1/2 inhibitor SCH772984 (3 or 6 mg/kg) or vehicle. Frozen sections were immunostained for phosphorylated ERK1/2 (p-ERK1/2) and the endothelial junctional protein VE-cadherin (VE-CAD) (A), or for endothelium (CD31, red), pericytes (NG2, green), and smooth muscle cells (α-SMA, cyan) (C), followed by quantification of the percentage of p-ERK1/2-positive endothelial cells (B) and of vessel diameters (D). ERK inhibition was effective with 6 mg/kg and completely prevented the vessel enlargement caused by sEphB4. *lumen of vascular enlargements. Scale bar = 20 μm. Mean ± SEM; $n = 4$ independent samples/group; * $P < 0.05$, ** $P < 0.01$, *** $P < 0.001$, and **** $P < 0.0001$ (one-way ANOVA with Bonferroni multiple comparisons test).
- E–G Muscles implanted as above were harvested after 2 weeks, while treating animals systemically with 6 mg/kg of SCH772984 or vehicle for the first 7 days. Frozen sections were immunostained for endothelium (CD31, red), pericytes (NG2, green), and smooth muscle cells (α-SMA, cyan) (E), followed by quantification of the percentage of vessel diameters (F) and vessel length density (G). ERK inhibition prevented the switch to aberrant angiogenesis caused by sEphB4, without impairing the amount of normal angiogenesis induced by V-low. Scale bar = 20 μm. Mean ± SEM; $n = 4$ independent samples/group; * $P < 0.05$, ** $P < 0.01$, *** $P < 0.001$, and **** $P < 0.0001$ (one-way ANOVA with Bonferroni multiple comparisons test).

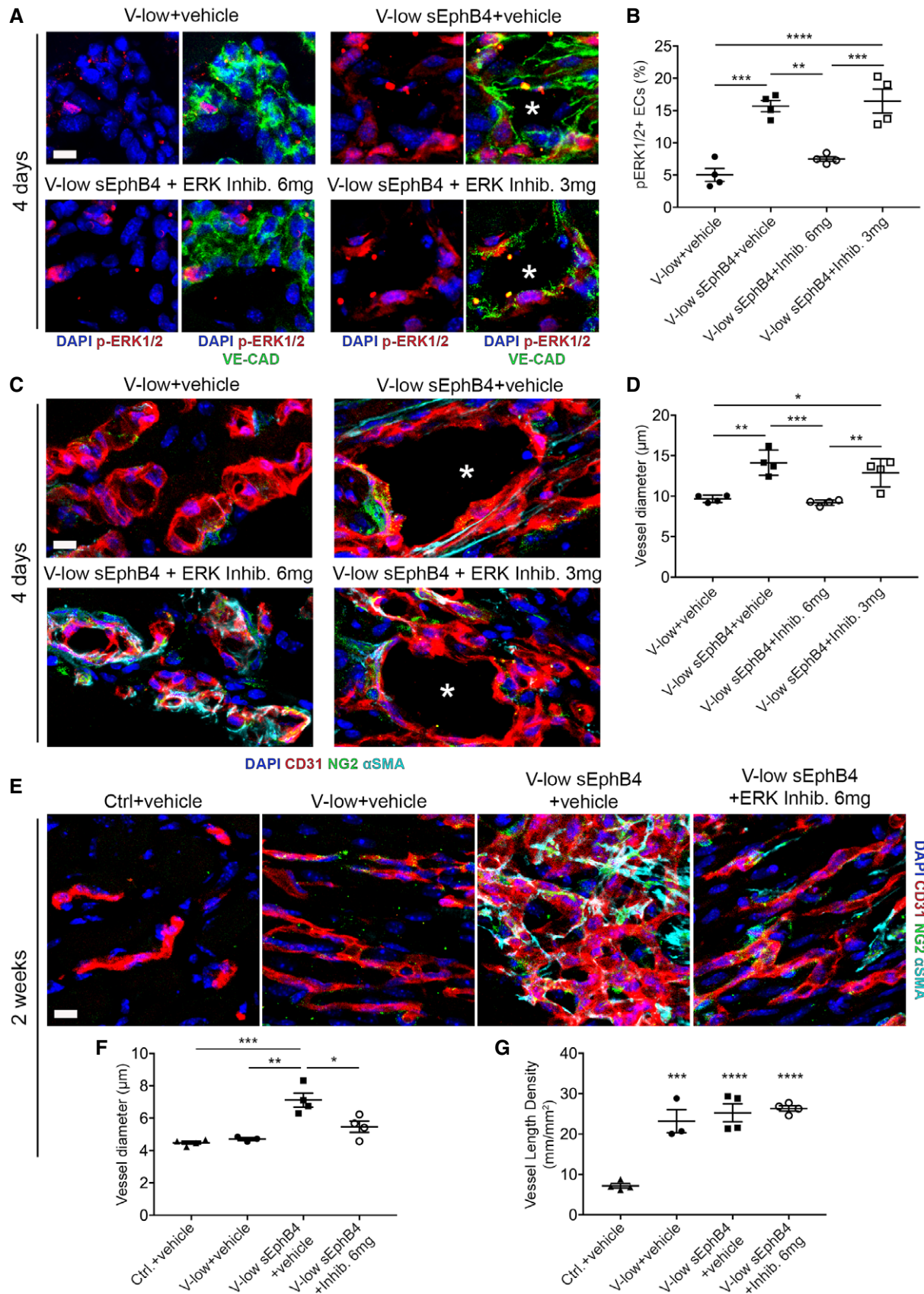


Figure 7.

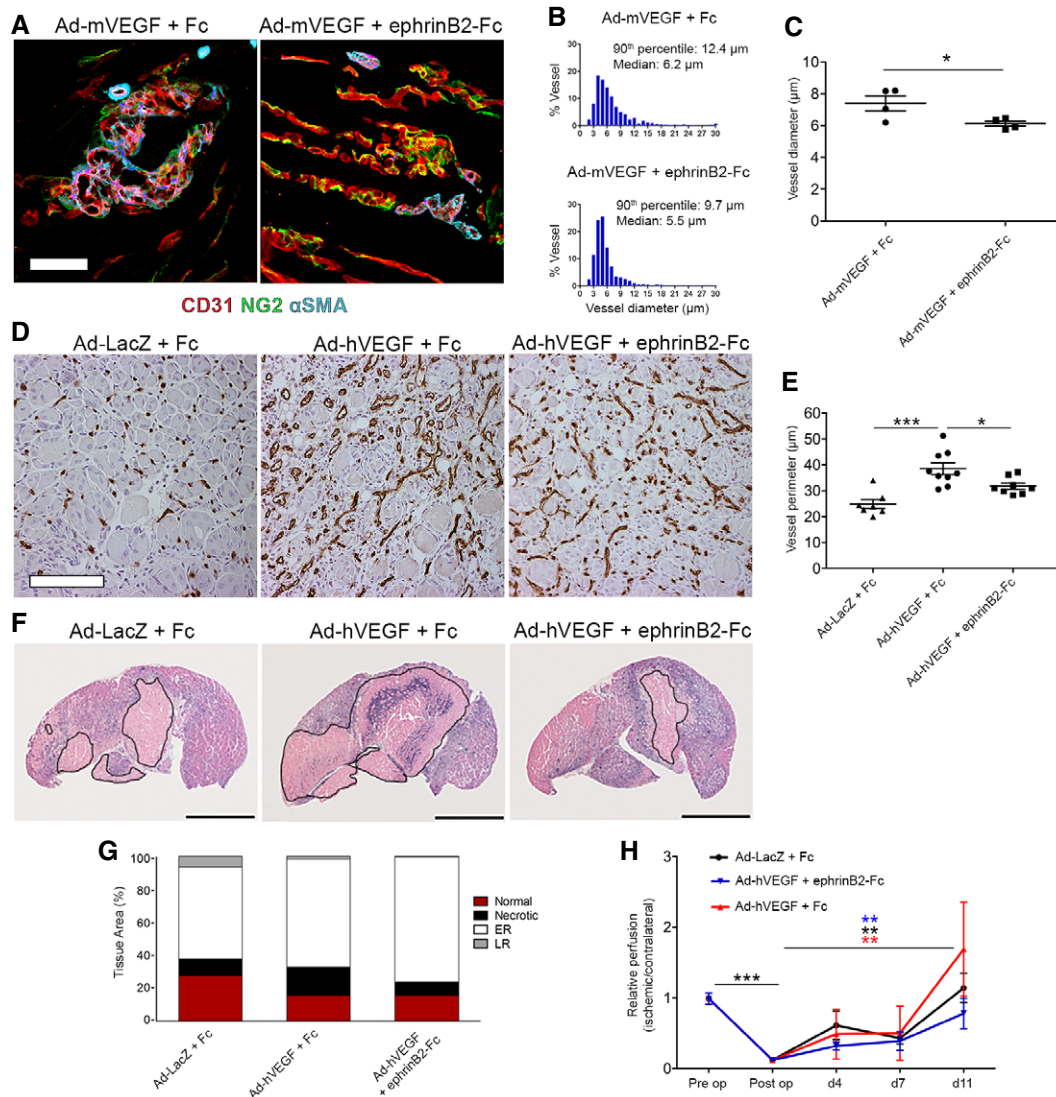


Figure 8. EphB4 stimulation prevents aberrant angiogenesis by uncontrolled adenoviral VEGF delivery both in normal and in ischemic muscle.

A–C Immune-deficient SCID mice received intramuscular injections of adenovirus expressing murine VEGF₁₆₄ (Ad-mVEGF) and were treated systemically with ephrinB2-Fc or control Fc proteins. Muscles were harvested 2 weeks later, and frozen sections were stained for endothelium (CD31, red), pericytes (NG2, green), and smooth muscle cells (α -SMA, cyan) (A). Vessel diameters were quantified, and results are shown as size distribution (B) and mean of individual measurements in each sample \pm SEM (C). EphB4 stimulation prevented the appearance of aberrantly enlarged and smooth muscle-covered vascular structures and reduced the average diameter of induced vessels. Scale bar = 50 μ m. $n = 4$ independent samples/group; * $P < 0.05$ (one-tailed t -test, after data normalization by logarithmic-transformation).

D–H Hindlimb ischemia was induced in immune-competent LDLR^{-/-}ApoB^{100/100} mice. Adenoviral vectors expressing human VEGF₁₆₅ (Ad-hVEGF) or control LacZ (Ad-LacZ) were delivered by intramuscular injection and animals received systemic treatment with ephrinB2-Fc or control Fc proteins. After 11 days, muscles were harvested and immunohistochemical staining for CD31 was performed to assess vessel morphology (D) and to quantify vascular size by measuring vessel perimeters (E), while tissue damage was quantified on H&E-stained sections (F, G), distinguishing tissue areas as normal, necrotic, early-, and late-regenerating (ER and LR, respectively). Blood flow was measured non-invasively by contrast-enhanced ultrasound (H) before and after surgery (pre-op and post-op, respectively) and after 4, 7, and 11 days (d4, d7, and d11) and is presented as the ratio of ischemic/contralateral normal leg of each animal. EphB4 stimulation prevented the appearance of aberrantly enlarged vascular lacunae and normalized the size of VEGF-induced vessels, while a non-significant trend was also observed toward reduced tissue necrosis, increased regeneration, and normalized blood flow. Scale bars = 100 μ m (D) and 2 mm (F). Mean \pm SEM; (D–G) $n = 7$ –9 independent samples/group; * $P < 0.05$ and *** $P < 0.001$ (one-way ANOVA and Bonferroni *post hoc* test); (H) $n = 4$ –10 animals/group; *** $P < 0.001$ post-op vs. pre-op, ** $P < 0.01$ post-op vs. day 11 Ad-LacZ, or vs. Ad-VEGF, or vs. Ad-VEGF + ephrinB2-Fc, according to the corresponding color (one-way ANOVA and Bonferroni multiple comparisons test).

(Fig 8D). Since ischemic tissue cannot be perfuse-fixed efficiently, vascular structures undergo variable degrees of collapse, making diameter or area measurements unreliable. Therefore, vascular size

was quantified by measuring vessel perimeters, which instead are less affected by collapse. EphrinB2-Fc significantly reduced the mean size of VEGF-induced vessels (Fig 8E; Ad-hVEGF + Fc =

$38.5 \pm 2.2 \mu\text{m}$ vs. Ad-hVEGF + ephrinB2-Fc = $31.8 \pm 1.2 \mu\text{m}$, $P < 0.05$; Ad-LacZ + Fc = $24.9 \pm 1.7 \mu\text{m}$), confirming the results in non-ischemic muscle. Functionally, although the aberrant vasculature can be highly perfused, it can have deleterious effects on muscle function and recovery from ischemia, for example, through the formation of arteriovenous shunts that actually reduce effective metabolic exchange in tissue [37]. In agreement with the normalization of vascular structure, ephrinB2-Fc treatment displayed a non-significant trend toward normalization of the *supra*-physiological perfusion increases induced by Ad-hVEGF (Fig 8H). A non-significant trend was also observed toward reduced ischemia-related muscle damage (necrotic area: Ad-hVEGF + Fc = $17.5 \pm 9.8\%$ vs. Ad-hVEGF + ephrinB2-Fc = $8.4 \pm 3.7\%$) and increased tissue regeneration (regenerating area: Ad-hVEGF + Fc = $65.2 \pm 9.2\%$ vs. Ad-hVEGF + ephrinB2-Fc = $75.4 \pm 7.5\%$), although spontaneous regeneration was significant (Ad-LacZ regenerating area = $55.8 \pm 12.1\%$) (Fig 8F and G). Taken together, these results suggest that EphB4 stimulation by systemic ephrinB2-Fc treatment is effective in controlling undesired vascular responses of VEGF gene delivery also under therapeutically relevant conditions.

Discussion

By complementary loss- and gain-of-function approaches, we have identified the EphB4 receptor as a key regulator of intussusceptive angiogenesis and a target to control the dose-dependent outcome of VEGF delivery to skeletal muscle. EphB4 activation by systemic treatment with recombinant ephrinB2-Fc protein effectively prevented aberrant vascular growth without interfering with normal angiogenesis, thereby promoting normal microvascular network formation despite high and uncontrolled VEGF doses. Mechanistically, EphB4 activity finely tuned the degree of endothelial proliferation induced by specific VEGF doses without affecting activation of VEGF-R2, but rather converging on its downstream signaling and tuning the phosphorylation of ERK1/2.

While sprouting requires a coordinated interplay between directed migration of tip cells and proliferation of stalk cells behind the tip [38], during intussusceptive angiogenesis pre-existing vessels initially undergo circumferential enlargement that entails exclusively endothelial proliferation without migration [6]. The degree of vascular enlargement is proportional to VEGF dose and determines the outcome of subsequent intussusceptive remodeling. In fact, intraluminal pillar formation is initiated with similar frequency with both low and high VEGF, but excessive diameters prevent their successful completion, leading to failure to split and progressive growth into angioma-like vascular structures [9]. Here, we identified EphB4 activation as a specific mechanism controlling the outcome of intussusceptive angiogenesis in adult skeletal muscle, by fine-tuning the endothelial proliferation induced by specific doses of VEGF and therefore controlling the degree of circumferential enlargement achieved before transluminal pillar formation and vessel splitting. It is interesting to note how the total amount of proliferating Ki67⁺ cells 3 days after VEGF delivery was similar with both low and high VEGF doses, in agreement with our previous findings [9], and it was not altered by EphB4 stimulation or inhibition (Fig 5A and C). Rather, both VEGF dose and EphB4 activity controlled the proportion of endothelial cells in the G2-M phase,

marked by the phosphorylation of histone H3 (Fig 5B and D), suggesting an effect on the speed of proliferation, that is, the frequency of transition from G1 to the S-G2-M phase, rather than on the re-entry into the cell cycle from quiescence, that is, the G0-G1 transition [22,23].

Pericyte recruitment to nascent vascular structures is crucial for normal morphogenesis, stabilization, and function of microvascular networks, through a complex array of signals with endothelial cells [21]. Pericyte loss by interference with PDGF-BB/PDGF-R β signaling by genetic means during development [39,40] or blockade during VEGF-induced angiogenesis in adult tissue [12] leads to unabated endothelial proliferation and the growth of aberrantly enlarged vascular structures, which are fragile and cause lethal hemorrhages. Despite the complexity of the pericyte-endothelial molecular cross-talk, here we provide evidence that the ephrinB2-EphB4 pathway is responsible for the pericyte function of regulating the switch between normal and aberrant angiogenesis by VEGF dose. In fact, the effects of EphB4 inhibition or stimulation reported here mimic closely the results obtained in a similar setting by blocking or promoting pericyte recruitment through manipulation of PDGF-BB signaling, respectively [12]. Interestingly, the observed lack of effect by TGF- β blockade by LAP overexpression is in agreement with our own recent results, showing that a blocking anti-TGF- β 1 antibody did not affect the normal angiogenesis induced by low VEGF, although it significantly impaired endothelial expression of Semaphorin3A and the recruitment of a pro-stabilizing monocyte population [41]. These results suggest non-overlapping roles for the two pathways in vascular morphogenesis and stabilization in the setting of intussusceptive angiogenesis.

EphrinB2/EphB4 signaling has well-established functions in arteriovenous differentiation, where ephrinB2 and EphB4 selectively mark the arterial and venous endothelium, respectively [42], and in sprouting angiogenesis. During sprouting, functions of the ephrinB2/EphB4 pathway have been ascribed most clearly to the ephrinB2 partner. In fact, ephrinB2 was found to localize on the filopodia of tip cells, where it stimulates their motility and sprout formation by increasing endocytosis and signal activity of both VEGF-R2 and VEGF-R3 [30,43], but it does not appear to affect endothelial proliferation during sprouting [30]. The role of EphB4, which is absent from the tips and expressed on cells behind the growing front, remains to be elucidated. On the other hand, EphB4 overexpression has been described to suppress sprouting and switch vascular growth to circumferential enlargement, but independently of its kinase activity and rather through stimulation of ephrinB2 reverse signaling [44]. In contrast, here we found that EphB4 forward signaling is crucial to regulate intussusceptive angiogenesis, which takes place essentially without migration and rather only through proliferation. In fact, treatment with monomeric sEphB4 not only inhibits activation of endogenous EphB4, but also interferes with ephrinB2 reverse signaling, by preventing interaction and productive multimerization of the two binding partners. While this would be expected to cause reduced VEGF-R2 activation and tip cell migration in the setting of sprouting, we rather observed an increase in the outcome of VEGF signaling specifically on proliferation through ERK1/2 phosphorylation during the process of circumferential enlargement and intussusception, in the absence of tip cells. Conversely, specific activation of

EphB4 by treatment with ephrinB2-Fc had the opposite effect, with reduction in ERK1/2 phosphorylation and endothelial proliferation, both *in vitro* and *in vivo*. Increased ERK1/2 activity was required downstream of EphB4 blockade. In fact, treatment with an ERK inhibitor prevented both excessive vascular enlargement and appearance of aberrant vascular structures, while normal angiogenesis was not impaired (Fig 7), mimicking the effects of EphB4 stimulation by ephrinB2-Fc in conditions of high VEGF. Taken together, these data suggest a complementary function for ephrinB2 to stimulate VEGF-induced tip cell migration in sprouting and for EphB4 to reduce VEGF-induced ERK1/2 phosphorylation and endothelial proliferation in the absence of tip cells during intussusceptive angiogenesis.

From a therapeutic perspective, it is particularly important that EphB4 stimulation did not completely abolish VEGF-induced endothelial proliferation, but rather only reduced it by about 40%, thereby preventing aberrant angiogenesis without interfering with normal vascular growth. This can be explained considering that VEGF-R2 stimulates endothelial proliferation through two parallel pathways, one through RAS and the other through PKC β , which then converge on the RAF-MEK-ERK1/2 cascade [45,46]. The major contributor to ERK1/2 activation by VEGF-R2 *in vivo* has been found to be the PKC β pathway, through recruitment of PLC γ upon phosphorylation of tyrosine Y1175/1173 [46]. However, while mutation of Y1175/1173 both abolished VEGF-induced ERK1/2 activation and caused embryonic lethality [47,48], global disruption of the *Prkcb* gene, encoding PKC β , did not cause major vascular phenotypes [49], showing that the control of ERK1/2 activation by VEGFR-2 is redundant downstream of Y1175/1173 phosphorylation. On the other hand, EphB4 directly binds and activates the RAS GTPase activating protein RASA1, which negatively regulates RAS activity through its GTPase function [50,51]. Therefore, by inhibiting one branch of a redundant circuit, EphB4 stimulation can achieve modulation of ERK1/2 activation and endothelial proliferation, while sparing sufficient activity to avoid disruption of vascular growth.

Controlling precisely the outcome of VEGF signaling for therapeutic purposes is a significant clinical challenge [52]. Recent findings show that delivery of an alternative ligand may activate VEGF-R2 more gently and with less stringent requirements for dose control. For example, VEGF-B binds VEGF-R1 and not VEGF-R2, but it has been found to effectively induce both cardiac angiogenesis and arteriogenesis by displacing R1-bound VEGF-A and making it available for signaling through R2 [53,54]. Since VEGF-R2 is activated only indirectly by endogenously available VEGF-A, even significant VEGF-B overexpression does not cause excessive stimulation of R2 signaling [54]. However, the vascular effects of VEGF-B appear restricted to the heart and its delivery does not induce any angiogenesis in skeletal muscle or other tissues [53].

The results reported here show that targeting a separate pathway that converges on downstream signaling provides a new paradigm to modulate VEGF-R2 output. Pharmacologic targeting of EphB4 can be achieved with systemic treatments offering significant translational potential, for example, in conjunction with VEGF gene therapy. The therapeutic potential of such approach remains to be established and will require further investigation in relevant large-animal pre-clinical models.

Materials and Methods

Construction of blocker retroviral vectors

Retroviral vectors were constructed encoding the following soluble blockers of TGF- β 1, Ang/Tie2, and ephrinB2/EphB4 signaling, respectively: (i) the latency-associated peptide (LAP), which associates with TGF- β 1 to form the non-functional latent TGF β complex, thereby inhibiting the biological activity of endogenous TGF- β 1 [55]; (ii) a receptor body formed by fusing a truncated version of the receptor Tie2 and the Fc portion of IgG immunoglobulin (sTie2Fc), which sequesters angiopoietins and prevents them from signaling [56]; and (iii) a monomeric truncated version of the receptor EphB4 (sEphB4), which binds membrane-bound ephrinB2 without activating it, as it does not form multimers, but prevents it from binding and activating the endogenous endothelial EphB4 receptor [57]. The cDNAs of human LAP, murine sTie2Fc, and human sEphB4 were cloned into the pAMFG retroviral vector in a bicistronic cassette [13], linked through an internal ribosomal entry sequence (IRES) to a truncated version of rabbit CD4 as a convenient cell surface marker, producing the pAMFG.CD4, pAMFG.CD4.LAP, pAMFG.CD4.sTie2Fc, and pAMFG.CD4.sEphB4 retroviral vectors.

Retroviral transduction of myoblasts

Primary myoblasts isolated from C57BL/6 mice were infected at high efficiency [58] with retroviruses carrying the cDNA of murine VEGF₁₆₄ linked through an internal ribosome entry sequence (IRES) to a truncated murine CD8a as a FACS-sortable marker, or only CD8 as controls [13]. Early-passage myoblast clones were isolated using a FACS Vantage SE cell sorter (Becton Dickinson, Basel, Switzerland) as described [13], in order to obtain populations in which every cell expressed the same VEGF level. V-low and control cells were further infected with retroviruses expressing LAP, sTie2Fc or sEphB4, or only CD4 as control. Transduced populations were FACS-sorted based on the staining for the CD4 surface marker to eliminate non-infected cells. All myoblast populations were cultured in 5% CO₂ on collagen-coated dishes, with a growth medium consisting of 40% F10, 40% low-glucose DMEM, 20% FBS, 1% penicillin/streptomycin, and 1% L-glutamine, supplemented with 2.5 ng/ml basic FGF, as previously described [59].

CD4 flow cytometric analysis

Expression of the truncated CD4 marker was assessed by staining myoblasts with a FITC-conjugated antibody against rabbit CD4 (clone MCA799F, AbD Serotec, Raleigh, USA), using 0.4 μ g of antibody/10⁶ cells in 200 μ l (1:50 dilution) of phosphate-buffered saline (PBS) with 5% BSA for 20 min on ice. Data were acquired using a FACS Calibur flow cytometer (Becton Dickinson) and analyzed using FlowJo software (Tree Star, Ashland, USA). Cell sorting was performed with a BD Influx cell sorter (Becton Dickinson).

Blocker expression by RT-PCR

Specific expression of the correct blockers in each myoblast population was verified by RT-PCR using primers specific for LAP (FW

5'-GCTGTGGCTACTGGTCTGA-3' and RV 5'-CCGGGAGCTTTGCA GATGCT-3'), sTie2Fc (FW 5'-GTGGAGTCAGCTTGCTCCTT-3' and RV 5'-TGCACACACAGCTCGTAGTC-3'), and sEphB4 (FW 5'-TTTGG AAGAGACCCTGCTGA-3' and RV 5'-CCGTTTCAGGCGGAAACC-3'). PCR was performed using HiFi PCR Premix (Takara Clontech, St-Germain-en-Laye, France) with 35 cycles of amplification consisting of denaturation at 98°C for 10 s, annealing at 55°C for 15 s, and extension 72°C for 10 s, on a Veriti Thermal Cycler (Applied Biosystems, Basel, Switzerland).

Blocker functional assays

LAP

A TGF- β reporter cell line was produced by transducing HEK293 cells with lentiviral vectors expressing luciferase under the control of a SMAD response element or a control minimal CMV promoter, according to the manufacturer's instructions (pGreenFire™ Transcription Reporters, System Biosciences, Mountain View, USA). Cells were seeded in 96-well plates at 50% confluency and cultured with high-glucose DMEM supplemented with 10% FBS, 1% penicillin/streptomycin, and 1% L-glutamine. After 12 h, medium was replaced with conditioned medium from either LAP or control CD4 myoblasts, which was previously incubated on ice for 30 min with different amounts of recombinant human TGF- β 1 (R&D Systems) and then warmed at 37°C for 15 min. After 24 h, medium was aspirated and cells were lysed on ice in 60 μ l of ice-cold lysis buffer for 15 min and luciferase activity was measured with the BrightGlo Luciferase Assay System (Promega, Madison, USA), according to manufacturer's instructions. Luminescence from reporter activation was measured for 1 s/well on a MicroLumatPlus luminometer (Berthold Technologies, Bad Wildbad, Germany).

sTie2Fc

The RAW264.7 macrophage cell line [60] was seeded in 24-well plates at the density of 100,000 cells/well and cultured with RPMI medium supplemented with 10% FBS, 1% penicillin/streptomycin, and 1% L-glutamine. For the assay, cells were incubated with conditioned medium from either sTie2Fc or control CD4 myoblasts that was previously kept on ice for 30 min with different amounts of recombinant COMP-Ang1 (AdipoGen, Liestal, Switzerland) and then warmed at 37°C for 15 min. After 60 min, conditioned medium was replaced with fresh RPMI containing 100 ng/ml of LPS, and after 24 h, cells were collected for RNA extraction.

sEphB4

Human umbilical vein endothelial cells (HUVEC) were seeded at the density of 500,000 cells/T25 flask and cultured overnight in M199 medium supplemented with 20% FBS, 100 μ g/ml endothelial cell growth supplement (Sigma-Aldrich, St. Louis, USA), 50 U/ml sodium heparin (Sigma-Aldrich), and 1% penicillin/streptomycin. Afterward, cells were incubated with conditioned medium from either sEphB4 or control CD4 myoblasts that was previously kept on ice for 30 min with 2 μ g/ml mouse ephrinB2-Fc (R&D Systems) pre-clustered with anti-Fc Ab [16] and then warmed at 37°C for 15 min. After 30 min, HUVEC were lysed and the amount of phospho-EphB4 was quantified using a human phosphotyrosine EphB4 ELISA kit (Raybiotech, Norcross, GA, USA) according to manufacturer's instructions.

VEGF₁₆₄ ELISA

The production of VEGF₁₆₄ in cell culture supernatants was quantified by a Quantikine mouse VEGF Immunoassay ELISA kit (R&D Systems, Abingdon, UK). One milliliter of fresh medium was incubated for 4 h on myoblasts seeded overnight in a 60-mm dish, filtered, and analyzed in duplicate. Results were normalized by the number of cells and time of incubation. Four dishes of cells were assayed per cell type ($n = 4$).

In vivo myoblast implantation

To avoid an immunological response to transduced myoblasts expressing xenogenic proteins (LacZ, rabbit CD4, human LAP, and sEphB4), immunodeficient SCID CB.17 mice (Charles River Laboratories, Sulzfeld, Germany) were used. Myoblasts were dissociated in trypsin and resuspended at a concentration of 10⁸ cells/ml in sterile PBS with 0.5% BSA (Sigma-Aldrich Chemie GmbH, Steinheim, Germany), and 10⁶ cells were injected into the *Tibialis anterior* (TA) and *gastrocnemius* (GC) muscles in the lower hindlimb, using a 30-gauge needle syringe, as previously described [10]. All experiments were performed with similar number of samples from both muscle locations, and the results were pooled together. Mice of 8–12 weeks of age, with equal representation of both genders, were randomly assigned to experimental groups, with a minimum of $n = 4$ mice/group.

Recombinant VEGF delivery by fibrin hydrogels

The transglutaminase substrate sequence NQEQVSPL (α 2-PI₁₋₈) was fused to the N terminus of the mouse VEGF-A₁₆₄ cDNA by PCR. The fusion protein was expressed into *Escherichia coli* strain BL21 (De3) pLys (Novagen, Madison, WI, USA) and isolated as described previously [61]. Fibrin matrices of optimized composition were prepared as previously described [17], incorporating 56 mg/ml of aprotinin- α 2-PI₁₋₈, to ensure controlled duration of degradation over 4 weeks, and 50 μ g/ml of α 2-PI₁₋₈-VEGF₁₆₄. For *in vivo* delivery, 6- to 8-week-old immunodeficient CB.17 SCID mice (Charles River Laboratories) were used to avoid an immunological response to human fibrinogen and cross-linking enzymes. A liquid volume of 50 μ l was aspirated rapidly with a 0.3-ml insulin syringe with integrated 30-gauge needle (Becton Dickinson, Basel, Switzerland) and injected into the GC muscle of the mice previously anesthetized with 3% isoflurane inhalation. After injection, *in situ* polymerization was allowed for 20 s before slowly extracting the needle.

Recombinant adenovirus production and in vivo implantation

Recombinant adenoviruses expressing mouse VEGF₁₆₄ or human VEGF₁₆₅ were produced using the Adeno-XTM Expression System (Clontech, Saint-Germain-en-Laye, France) according to the manufacturer's recommendations. Adenoviral vectors were diluted in physiological solution and injected in TA and GC muscles in the lower hindlimb of immune-deficient CB.17 SCID mice (Charles River Laboratories) at the titer of 1×10^8 infectious units/injection, with a 30-gauge needle syringe, as previously described [41]. Information on ischemia experiments is provided below.

EphrinB2-Fc treatment

To stimulate EphB4 signaling *in vivo*, mice received 1 mg/kg of mouse ephrinB2-Fc (R&D Systems) or control Fc (Abcam, Cambridge, UK) by intraperitoneal injections twice weekly, starting 3 days before the myoblast injection, according to published protocols [62].

ERK inhibitor treatment

To inhibit ERK1/2 activity *in vivo*, mice were treated with the selective and potent ERK inhibitor SCH772984 (Selleckchem, Lubio-Science, Zürich, Switzerland). Mice received 3, 6, or 12.5 mg/kg of the inhibitor or vehicle by intraperitoneal injections twice daily for 4 or 7 days, as published [34].

RNA extraction and quantitative real-time PCR

For RNA extraction from total muscles, freshly harvested tissue was frozen in liquid nitrogen and disrupted using a Qiagen Tissue Lyser (Qiagen, Basel, Switzerland) in 1 ml TRIzol reagent (Invitrogen, Basel, Switzerland) for 100 mg of tissue. Total RNA was isolated from lysed tissues or *in vitro* cultured myoblasts, RAW264.7, and human dermal microvascular endothelial cells (HDMEC) with an RNeasy Mini Kit (Qiagen) according to manufacturer's instruction. RNA was reverse transcribed into cDNA using the Omniscript Reverse Transcription kit (Qiagen) at 37°C for 60 min. Quantitative real-time PCR (qRT-PCR) was performed on an ABI 7300 Real-Time PCR system (Applied Biosystems, Basel, Switzerland). Expression of genes of interest was determined using the following TaqMan Gene Expression assays (Applied Biosystems) according to manufacturer's instructions: mouse *Tnfa* (Mm00443258_m1); mouse *Gapdh* (Mm03302249_g1); mouse *Pdgfb* (Mm00440678_m1); mouse *Pdgfrb* (Mm00435545_m1); mouse *Fgf2* (Mm01285715_m1); mouse *Vegfa* (Mm00437306_m1); human *Igf1* (Hs00365742_g1); human *Esm1* (Hs00199831_m1); and human *Gapdh* (Hs02758991_g1). In order to quantify endogenous *Vegfa* transcripts separately from those from the transduced myoblasts, a previously designed sets of primers and probe were used to detect a sequence on the mRNA 5'-UTR, which is absent from the vector-encoded transcripts [63]. Reactions were performed in triplicate for each template, averaged, and normalized to expression of the same-species *Gapdh* house-keeping gene.

Immunofluorescence tissue staining

Mice were anesthetized with ketamine (100 mg/kg) and xylazine (10 mg/kg) and sacrificed by intravascular perfusion of 1% paraformaldehyde in PBS pH 7.4. TA and GC muscles were harvested, post-fixed in 0.5% paraformaldehyde in PBS for 2 h, cryoprotected in 30% sucrose in PBS overnight at 4°C, embedded in OCT compound (CellPath, Newtown, Powys, UK), frozen in isopentane, and cryosectioned. The areas of engraftment were identified by tracking implanted myoblasts by X-gal staining (20- μ m sections) or adenoviral infection sites by the typical mononuclear infiltrate with H&E (10- μ m sections) in adjacent serial sections, as described previously [10]. For immunofluorescence staining, 10- μ m tissue sections were stained with the following

primary antibodies and dilutions: rat monoclonal anti-mouse CD31 (clone MEC 13.3, BD Biosciences, Basel, Switzerland) at 1:100; mouse monoclonal anti-mouse α -SMA (clone 1A4, MP Biomedicals, Basel, Switzerland) at 1:400; rabbit polyclonal anti-NG2 (Merck Millipore, Darmstadt, Germany) at 1:200; rat monoclonal anti-VE-cadherin (clone 11D4.1, BD Biosciences, Basel, Switzerland) at 1:200; rat monoclonal anti-mouse endomucin (clone V.7C7, Santa Cruz Biotechnologies, Santa Cruz, CA, USA) at 1:100; goat polyclonal anti-mouse podocalyxin (R&D Systems) at 1:100; rabbit polyclonal anti-Ki67 (Abcam, Cambridge, UK) at 1:100; rabbit polyclonal anti-laminin (Abcam) at 1:200; rabbit polyclonal anti-pHH3-Ser28 (Cell Signaling Technology, Danvers, USA) at 1:100; and goat polyclonal anti-EphB4 at 1:50 (R&D Systems). Fluorescently labeled secondary antibodies (Invitrogen) were used at 1:200.

For pERK1/2 staining, tissue sections were permeabilized with ice-cold methanol for 10 min and blocked with 5% goat serum and 2% BSA in PBS with 0.3% Triton X for 1 h at RT. Rabbit monoclonal anti-phospho-ERK1/2 antibody (Thr202/Tyr204, clone D13.14.4E, Cell Signaling Technology) was used at 1:100.

To study vessel perfusion, 100 μ g of FITC-labeled *Lycopersicon esculentum* lectin in 50 μ l (Vector Laboratories, Burlingame, USA) was injected into the femoral vein and allowed to circulate for 4 min before intravascular perfusion with 1% paraformaldehyde and muscle collection as described above.

Vascular analyses

Qualitative analysis of vascular morphology in immunofluorescence images was performed on all vascular structures visible in at least three fields/section with a 40 \times objective on a Carl Zeiss LSM710 3-laser scanning confocal microscope (Carl Zeiss, Feldbach, Switzerland) in at least five sections/muscle, cut at 100–150 μ m of distance from each other ($n = 4$ muscles/group). All histological analyses were performed by blinded investigators.

Vessel diameters were measured in fluorescently immunostained sections as described (Ozawa JCI 2004). Briefly, 10–20 fields/muscle ($n = 4$ muscles/group) were analyzed, measuring a total of minimum 300 diameters/group. Captured microscopic images were overlaid with a square grid, squares were randomly chosen, and the diameter of each vessel (if any) in the center of selected squares was measured. To avoid selection bias, the shortest diameter in the selected vascular segment was systematically measured. All images were taken with a 20 \times objective on an Olympus BX63 microscope (Olympus, Volketswil, Switzerland), and analyses were performed with Cell Sens software (Olympus).

Vessel length density (VLD) was quantified in fluorescently immunostained cryosections as described [10]. Briefly, 10–15 fields per muscle ($n = 4$ muscles/group) were analyzed by tracing the total length of vessels in the acquired field and dividing it by the area of the fields.

The quantification of mural cell coverage was performed on sections of leg muscles after immunostaining for endothelium (CD31), pericytes (NG2), and smooth muscle (α -SMA). The areas occupied by their respective signals were measured by Imaris 7.6.5 software (Bitplane, Zürich, Switzerland) on Z-Stack, 1,024 \times 1,024, 8-bit Fluorescence images acquired with 40 \times objective on a Carl Zeiss LSM710 3-laser scanning confocal microscope (Carl Zeiss,

Feldbach, Switzerland), and the coverage indexes were calculated as the ratio between the values of NG2 or α -SMA and CD31.

Ki67⁺ and pHH3⁺ endothelial cells were quantified as a percentage of all endothelial cells in analyzed vascular structures. 300–3,000 endothelial cells were analyzed/group in 3–5 fields taken from each area of effect. At least five areas with a clear angiogenic effect were analyzed per group ($n = 4$ muscles/group).

HDMEC *in vitro* assays

Human microvascular endothelial cells (HDMEC) were isolated as previously described [64] and cultured in endothelial cell basal medium (EBM, Vitaris, Baar, Switzerland) supplemented with 10% FBS, 1% penicillin/streptomycin, 10 μ g/ml sodium heparin, and 2.5 ng/ml FGF-2. Before each assay, cells were starved in EBM with 1% FBS for 2 h.

Flow cytometry analysis was performed with the following antibodies and dilutions: PE-conjugated mouse anti-VE-cadherin (clone BV9, Biolegend, San Diego, CA, USA) and PE-Cy7-conjugated rat anti-CD31 (clone 390, Biolegend) at 1:100; goat anti-EphB4; and goat anti-ephrinB2 (R&D Systems) at 1:50.

Cell cycle analysis

100,000 HDMEC were seeded in p60 dishes overnight and then stimulated with different combinations of the following reagents: 50 ng/ml hVEGF₁₆₅ (R&D Systems), 50 ng/ml or 2 μ g/ml ephrinB2-Fc (R&D Systems), and 25 ng/ml FGF-2 (BD Biosciences). After 24 h, cells were collected, fixed, and permeabilized with the FOXP3 Fix/Perm kit (Biolegend) according to the manufacturer's instructions, stained with rabbit polyclonal anti-Ki67 (Abcam), detected with an Alexa546-anti-rabbit secondary (Invitrogen), and with Alexa647-anti-pHH3 (clone HTA28, Biolegend). Finally, cells were incubated with Hoechst 33342 (Life Technologies, Zug, Switzerland) for 2 h in the dark at 4°C and analyzed with a Fortessa FACS analyzer (Becton Dickinson).

Receptor internalization assay by FACS

50,000 HDMEC were seeded in 6-well plate overnight and then stimulated with different combinations of the following reagents: 50 ng/ml hVEGF₁₆₅, 2 μ g/ml ephrinB2Fc, and 30 μ M axitinib (Tocris Bioscience, Bristol, UK) [29]. After 30 min of stimulation, cells were collected and stained for surface and total VEGF-R2, as previously described [65]. Briefly, non-fixed and non-permeabilized HDMEC were first stained with Alexa647-anti-VEGFR2 (clone HKDR-1; Biolegend) to label only the surface receptor. Subsequently, cells were fixed and permeabilized with the FOXP3 Fix/Perm buffer (Biolegend) and were split into two tubes, where one half was stained again with PE-anti-VEGFR2 (clone 7D4-6, Biolegend) in FOXP3 Perm buffer to visualize total cellular VEGFR2, while the other half was not stained. Analysis was performed with a Fortessa FACS analyzer (Becton Dickinson).

Receptor internalization assay by Western blot

Protection of VEGF-R2 from extracellular trypsin treatment was exploited in the quantification of the internalized VEGF-R2. HDMEC were grown to sub-confluency in 6-well plates and then stimulated with 50 ng/ml hVEGF₁₆₅, with or without addition of 2 μ g/ml ephrinB2Fc. After 30 min of stimulation, cells were

washed with ice-cold PBS and incubated on ice for 30 min with freshly prepared trypsin (1 mg/ml, Amimed-Bioconcept) to cleave VEGF-R2 molecules exposed on the cell surface. The enzymatic cleavage reaction was quenched by addition of soybean trypsin inhibitor (1 mg/ml, Sigma). Cultures were rinsed and lysed in NP-40 buffer containing 25 mM Tris-HCl (pH 7.4), 150 mM NaCl, 1% NP-40, 1 mM EDTA, 5% glycerol, phosphatase inhibitor cocktail, and protease inhibitor cocktail (both from Roche Diagnostics, Switzerland). Lysates (10 μ g protein/lane) were analyzed by SDS-PAGE and Western blot using an anti-VEGF-R2 antibody (Cell Signaling Technology, CST #2479). An anti-GAPDH antibody (Abcam, Cambridge, UK) was used as protein loading control. Secondary HRP-conjugated anti-species specific IgGs were from Southern Biotechnology (BioReba AG, Reinach, Switzerland). Signal detection was performed using the Bio-Rad Molecular Imager Gel Doc XR⁺ system (Bio-Rad Laboratories, Hercules, CA, USA), and densitometric quantification was performed using Image Lab software (Bio-Rad). Two replicate wells were used for each experimental condition.

Phosphorylation assay

10,000–15,000 HDMEC were cultured in 8-well culture slides (Corning) and stimulated with 50 ng/ml hVEGF₁₆₅ and 2 μ g/ml ephrinB2-Fc alone or together for 10 min. Cells were immediately washed with PBS, fixed with 4% paraformaldehyde in PBS, blocked with 5% goat serum and 2% BSA in PBS with 0.3% Triton X for 1 h at RT, and stained with a rabbit monoclonal anti-phosphoTyr1175-VEGF-R2 antibody (clone D5B11, Cell Signaling Technology) and a goat anti-VE-cadherin (C-19, Santa Cruz Biotechnology, Santa Cruz, CA, USA), both at 1:200, followed by secondary antibody detection as described above. All samples were batch-stained together with same master mix of antibodies. In order to quantify the amount of phosphoVEGF-R2, stained cells were analyzed on a LSM710 3-laser scanning confocal microscope (Carl Zeiss), acquiring 8-bit images (Z-Stack, 1,024 \times 1,024) with a 40 \times objective, and maintaining the same acquisition settings for all samples. The amount of phosphoVEGF-R2 protein was measured by quantifying the staining intensity and normalized by the endothelial volume from the VE-cadherin staining, using the Imaris 7.6.4 software (Bitplane, Zürich, Switzerland) to measure total pixel intensity of endothelial-specific phosphoVEGF-R2 immunostaining.

Hindlimb ischemia, gene transfer, and analysis

Immune-competent genetically hyperlipidemic female LDLR^{-/-} ApoB^{100/100} mice (age of 14–17 months, $n = 28$), which are deficient for the LDL receptor and express only apolipoprotein B100 in C57Bl/6J genetic background [36], were fed on a standard chow diet. Experimental unilateral hindlimb ischemia was induced by permanent ligation of both common femoral artery and vein proximal to the origin of the profound femoral artery branch. Post-operatively, the posterior calf muscles received intramuscular injections of 2×10^{10} pfu/ml adenoviral vectors expressing either human VEGF-A₁₆₅ (Ad-hVEGF) or beta-galactosidase (Ad-LacZ) as a control. Mice were treated with i.p. injections of ephrinB2-Fc (R&D Systems) or control Fc (Abcam) as described above 0, 3, 6, and 9 days after the gene transfer. All animals were assigned to the different treatment groups by randomization before surgery.

Contrast-enhanced ultrasound imaging of perfusion and data analysis

To follow muscle perfusion recovery after ischemia, contrast-enhanced ultrasound imaging (CEU) was performed pre-operatively and 0, 4, 7, and 11 days post-operation with a Siemens Acuson Sequoia 512 system equipped with a 15L8 transducer using the Cadence contrast pulse sequencing (CPS) imaging mode with the following parameters: frequency 14 MHz, power -8 dB, mechanical index 0.25, CPS gain 0, and depth 20 mm [66]. Transverse plane perfusion video clips of both ischemic and intact hindlimbs were recorded upon the administration of an intravenous bolus injection of 50 μ l of Sonovue contrast agent (Bracco, Milano, Italy) via the jugular vein. Maximal signal intensity (dB) of the video clips, representing relative perfusion, was quantified with Datapro software v2.13 (Noesis, Courtaboeuf, France), and signal intensity–time curves were created ($n = 4$ –10 animals/group).

Histological analyses

Animals were sacrificed on day 11. Posterior calf muscles were collected for histological analysis after perfusion–fixation with 1% paraformaldehyde. Muscle samples were further immersed for 4 h in 4% paraformaldehyde–sucrose and then in 15% sucrose before paraffin embedding. Four- μ m-thick transversely cut sections were used to analyze muscle tissue damage by H&E staining and vascularity by CD31 immunohistochemistry. For tissue damage assessment, four different histological muscle areas were classified on H&E-stained sections as: (i) normal; (ii) necrotic (myofibers with no nuclei); (iii) early regeneration (appearance of basophilic satellite cells), or (iv) late regeneration (eosinophilic myofibers with angular shape and centrally positioned nuclei). Each corresponding muscle area was quantified using analySIS imaging software (Soft Imaging System GmbH, Münster, Germany) and expressed as a percentage of the whole cross-sectional muscle area ($n = 7$ –9 animals/group).

Vascularity was assessed by immunohistochemical staining with a rat monoclonal anti-mouse CD31 primary antibody (clone MEC 13.3, BD Biosciences Pharmingen, dilution 1:25, overnight at $+4^{\circ}\text{C}$), with blocking in 10% rabbit serum, 2% mouse serum, and 1% BSA 1 h at RT, followed by a biotinylated rabbit anti-rat secondary antibody (BA-4001, Vector laboratories, dilution 1:200, 30 min at RT) and detection with the avidin–biotin–horseradish peroxidase system (Vector Laboratories) with tyramide signal amplification (TBA, Biotin System, PerkinElmer, Shelton, USA) and DAB as a chromogen (Zymed, San Francisco, USA). Micrographs of the stained sections were acquired with $200\times$ magnification using an Olympus AX-70 light microscope (Olympus Optical, Tokyo, Japan) and analySIS imaging software (Soft Imaging System GmbH). Perimeters of all visible vessels were quantified from five fields/sample of CD31-stained sections acquired within regenerating muscle tissue in a standardized way ($n = 7$ –9 muscles/group), using Cell Sens software (Olympus). All measurements were performed by a blinded observer.

Statistics

Data are presented as mean \pm standard error. The significance of differences was assessed with the GraphPad Prism 6 software (GraphPad Software). The normal distribution of all data sets was tested and, depending on the results, multiple comparisons were performed with the parametric one-way analysis of variance

(ANOVA) followed by the Bonferroni test, or with the nonparametric Kruskal–Wallis test followed by Dunn's post-test, while single comparisons were analyzed with the nonparametric Mann–Whitney test or the parametric one-tailed *t*-test. Gene expression data representing fold-changes vs. control, which are asymmetrically distributed, were first normalized by logarithmic-transformation and then analyzed by one-way ANOVA followed by the Bonferroni test for multiple comparisons, or by *t*-test with Welch's correction for single comparisons. Vessel diameter values were first normalized by \log_2 -transformation and then analyzed by one-way ANOVA followed by Bonferroni test for multiple comparisons or by one-tailed *t*-test for single comparisons. $P < 0.05$ was considered statistically significant.

Study approval

Animal studies were performed in accordance with the Swiss Federal guidelines for animal welfare and were approved by the Veterinary Office of the Canton of Basel-Stadt (Basel, Switzerland; Permit 2071). All experimental procedures for ischemia studies in $\text{LDLR}^{-/-}$ – $\text{ApoB}^{100/100}$ mice were approved by the National Animal Experiment Board of Finland (license number: ESAVI/5343/04.10.07/2014) and carried out in accordance with the guidelines of the Finnish Act on Animal Experimentation.

Expanded View for this article is available online.

Acknowledgements

We would like to thank J.A. Hubbell and P. Briquez (University of Chicago, IL, USA) for providing recombinant aprotinin- $\alpha 2$ - PI_{1-8} and $\alpha 2$ - PI_{1-8} -VEGF₁₆₄. Human dermal microvascular endothelial cells (HDMEC) were a generous gift by James Kirkpatrick (Johannes Gutenberg University, Mainz, Germany). This work was supported by grants from the Swiss National Science Foundation (143898 and 163202), the Swiss Heart Foundation, the Basel Translational Medicine Hub and the EU FP7 Marie Curie grant AngioMatTrain (317304) to A.B., by a Swiss Heart Foundation grant to R.G.B., by grants from the Stiftung für Herz- und Kreislaufkrankheiten (Switzerland), the Swiss Heart Foundation and the Swiss National Science Foundation (159589) to M.F., by the Finnish Academy Center of Excellence in Cardiovascular and Metabolic Diseases and by the ERC grant CleverGenes to S.Y.H.

Author contributions

EG designed and performed experiments, analyzed data, and wrote/ commented on the manuscript; SB designed and performed experiments, analyzed data, and wrote/commented on the manuscript; AU designed and performed experiments, analyzed data and wrote/commented on the manuscript; GW designed and performed experiments, analyzed data, and wrote/ commented on the manuscript; PK-P designed and performed experiments, analyzed data and wrote/commented on the manuscript; MF designed and performed experiments and analyzed data; BD performed experiments and analyzed data; VS performed experiments; MGM designed and performed experiments and analyzed data; MT performed experiments; SR performed experiments; RG-B designed and performed experiments, analyzed data, and provided funding; SY-H designed experiments, wrote/commented on the manuscript, and provided funding; AB designed experiments, analyzed data, wrote/commented on the manuscript, and provided funding.

Conflict of interest

The authors declare that they have no conflict of interest.

References

- Folkman J (2007) Angiogenesis: an organizing principle for drug discovery? *Nat Rev Drug Discov* 6: 273–286
- Annex BH (2013) Therapeutic angiogenesis for critical limb ischaemia. *Nat Rev Cardiol* 10: 387–396
- Giacca M, Zacchigna S (2012) VEGF gene therapy: therapeutic angiogenesis in the clinic and beyond. *Gene Ther* 19: 622–629
- Yla-Herttuala S, Bridges C, Katz MG, Korpisalo P (2017) Angiogenic gene therapy in cardiovascular diseases: dream or vision? *Eur Heart J* 38: 1365–1371
- Potente M, Gerhardt H, Carmeliet P (2011) Basic and therapeutic aspects of angiogenesis. *Cell* 146: 873–887
- Gianni-Barrera R, Trani M, Reginato S, Banfi A (2011) To sprout or to split? VEGF, Notch and vascular morphogenesis. *Biochem Soc Trans* 39: 1644–1648
- Carmeliet P, Jain RK (2011) Molecular mechanisms and clinical applications of angiogenesis. *Nature* 473: 298–307
- De Spiegelaere W, Casteleyn C, Van den Broeck W, Plendl J, Bahramsoltani M, Simoens P, Djonov V, Cornillie P (2012) Intussusceptive angiogenesis: a biologically relevant form of angiogenesis. *J Vasc Res* 49: 390–404
- Gianni-Barrera R, Trani M, Fontanellaz C, Heberer M, Djonov V, Hlushchuk R, Banfi A (2013) VEGF over-expression in skeletal muscle induces angiogenesis by intussusception rather than sprouting. *Angiogenesis* 16: 123–136
- Ozawa CR, Banfi A, Glazer NL, Thurston G, Springer ML, Kraft PE, McDonald DM, Blau HM (2004) Microenvironmental VEGF concentration, not total dose, determines a threshold between normal and aberrant angiogenesis. *J Clin Invest* 113: 516–527
- von Degenfeld G, Banfi A, Springer ML, Wagner RA, Jacobi J, Ozawa CR, Merchant MJ, Cooke JP, Blau HM (2006) Microenvironmental VEGF distribution is critical for stable and functional vessel growth in ischemia. *FASEB J* 20: 2657–2659
- Banfi A, von Degenfeld G, Gianni-Barrera R, Reginato S, Merchant MJ, McDonald DM, Blau HM (2012) Therapeutic angiogenesis due to balanced single-vector delivery of VEGF and PDGF-BB. *FASEB J* 26: 2486–2497
- Misteli H, Wolff T, Fluglister P, Gianni-Barrera R, Gurke L, Heberer M, Banfi A (2010) High-throughput flow cytometry purification of transduced progenitors expressing defined levels of vascular endothelial growth factor induces controlled angiogenesis *in vivo*. *Stem Cells* 28: 611–619
- Horvat R, Hovorka A, Dekan G, Poczewski H, Kerjaschki D (1986) Endothelial cell membranes contain podocalyxin—the major sialoprotein of visceral glomerular epithelial cells. *J Cell Biol* 102: 484–491
- Kullander K, Klein R (2002) Mechanisms and functions of Eph and ephrin signalling. *Nat Rev Mol Cell Biol* 3: 475–486
- Noren NK, Foos G, Hauser CA, Pasquale EB (2006) The EphB4 receptor suppresses breast cancer cell tumorigenicity through an Abl-Crk pathway. *Nat Cell Biol* 8: 815–825
- Sacchi V, Mittermayr R, Hartinger J, Martino MM, Lorentz KM, Wolbank S, Hofmann A, Largo RA, Marschall JS, Groppa E et al (2014) Long-lasting fibrin matrices ensure stable and functional angiogenesis by highly tunable, sustained delivery of recombinant VEGF164. *Proc Natl Acad Sci USA* 111: 6952–6957
- Schense JC, Bloch J, Aebischer P, Hubbell JA (2000) Enzymatic incorporation of bioactive peptides into fibrin matrices enhances neurite extension. *Nat Biotechnol* 18: 415–419
- Schense JC, Hubbell JA (1999) Cross-linking exogenous bifunctional peptides into fibrin gels with factor XIIIa. *Bioconjug Chem* 10: 75–81
- Baffert F, Le T, Sennino B, Thurston G, Kuo CJ, Hu-Lowe D, McDonald DM (2006) Cellular changes in normal blood capillaries undergoing regression after inhibition of VEGF signaling. *Am J Physiol Heart Circ Physiol* 290: H547–H559
- Armulik A, Genove G, Betsholtz C (2011) Pericytes: developmental, physiological, and pathological perspectives, problems, and promises. *Dev Cell* 21: 193–215
- Scholzen T, Gerdes J (2000) The Ki-67 protein: from the known and the unknown. *J Cell Physiol* 182: 311–322
- Crosio C, Fimia GM, Loury R, Kimura M, Okano Y, Zhou H, Sen S, Allis CD, Sassone-Corsi P (2002) Mitotic phosphorylation of histone H3: spatio-temporal regulation by mammalian Aurora kinases. *Mol Cell Biol* 22: 874–885
- Nielsen PS, Riber-Hansen R, Jensen TO, Schmidt H, Steiniche T (2013) Proliferation indices of phosphohistone H3 and Ki67: strong prognostic markers in a consecutive cohort with stage I/II melanoma. *Mod Pathol* 26: 404–413
- Sahni A, Francis CW (2004) Stimulation of endothelial cell proliferation by FGF-2 in the presence of fibrinogen requires alphavbeta3. *Blood* 104: 3635–3641
- Makanya AN, Stauffer D, Ribatti D, Burri PH, Djonov V (2005) Microvascular growth, development, and remodeling in the embryonic avian kidney: the interplay between sprouting and intussusceptive angiogenic mechanisms. *Microsc Res Tech* 66: 275–288
- Simons M (2012) An inside view: VEGF receptor trafficking and signaling. *Physiology (Bethesda)* 27: 213–222
- Eichmann A, Simons M (2012) VEGF signaling inside vascular endothelial cells and beyond. *Curr Opin Cell Biol* 24: 188–193
- Hu-Lowe DD, Zou HY, Grazzini ML, Hallin ME, Wickman GR, Amundson K, Chen JH, Rewolinski DA, Yamazaki S, Wu EY et al (2008) Nonclinical antiangiogenesis and antitumor activities of axitinib (AG-013736), an oral, potent, and selective inhibitor of vascular endothelial growth factor receptor tyrosine kinases 1, 2, 3. *Clin Cancer Res* 14: 7272–7283
- Sawamiphak S, Seidel S, Essmann CL, Wilkinson GA, Pitulescu ME, Acker T, Acker-Palmer A (2010) Ephrin-B2 regulates VEGFR2 function in developmental and tumour angiogenesis. *Nature* 465: 487–491
- Rennel E, Mellberg S, Dimberg A, Petersson L, Botling J, Ameer A, Westholm JO, Komorowski J, Lassalle P, Cross MJ et al (2007) Endocan is a VEGF-A and PI3K regulated gene with increased expression in human renal cancer. *Exp Cell Res* 313: 1285–1294
- Schweighofer B, Testori J, Sturtzel C, Sattler S, Mayer H, Wagner O, Bilban M, Hofer E (2009) The VEGF-induced transcriptional response comprises gene clusters at the crossroad of angiogenesis and inflammation. *Thromb Haemost* 102: 544–554
- Sivaprasad U, Fleming J, Verma PS, Hogan KA, Desury G, Cohick WS (2004) Stimulation of insulin-like growth factor (IGF) binding protein-3 synthesis by IGF-I and transforming growth factor-alpha is mediated by both phosphatidylinositol-3 kinase and mitogen-activated protein kinase pathways in mammary epithelial cells. *Endocrinology* 145: 4213–4221
- Morris EJ, Jha S, Restaino CR, Dayananth P, Zhu H, Cooper A, Carr D, Deng Y, Jin W, Black S et al (2013) Discovery of a novel ERK inhibitor with activity in models of acquired resistance to BRAF and MEK inhibitors. *Cancer Discov* 3: 742–750
- Dai Y, Schwarz EM, Gu D, Zhang WW, Sarvetnick N, Verma IM (1995) Cellular and humoral immune responses to adenoviral vectors containing factor IX gene: tolerization of factor IX and vector antigens allows for long-term expression. *Proc Natl Acad Sci USA* 92: 1401–1405

36. Leppanen P, Koota S, Kholova I, Koponen J, Fieber C, Eriksson U, Alitalo K, Yla-Herttuala S (2005) Gene transfers of vascular endothelial growth factor-A, vascular endothelial growth factor-B, vascular endothelial growth factor-C, and vascular endothelial growth factor-D have no effects on atherosclerosis in hypercholesterolemic low-density lipoprotein-receptor/apolipoprotein B48-deficient mice. *Circulation* 112: 1347–1352
37. Zacchigna S, Tasciotti E, Kusmic C, Arsic N, Sorace O, Marini C, Marzullo P, Pardini S, Petroni D, Pattarini L et al (2007) *In vivo* imaging shows abnormal function of vascular endothelial growth factor-induced vasculature. *Hum Gene Ther* 18: 515–524
38. Gerhardt H, Golding M, Fruttiger M, Ruhrberg C, Lundkvist A, Abramsson A, Jeltsch M, Mitchell C, Alitalo K, Shima D et al (2003) VEGF guides angiogenic sprouting utilizing endothelial tip cell filopodia. *J Cell Biol* 161: 1163–1177
39. Hellstrom M, Gerhardt H, Kalen M, Li X, Eriksson U, Wollburg H, Betsholtz C (2001) Lack of pericytes leads to endothelial hyperplasia and abnormal vascular morphogenesis. *J Cell Biol* 153: 543–553
40. Lindahl P, Johansson BR, Leveen P, Betsholtz C (1997) Pericyte loss and microaneurysm formation in PDGF-B-deficient mice. *Science* 277: 242–245
41. Groppa E, Brkic S, Bovo E, Reginato S, Sacchi V, Di Maggio N, Muraro MG, Calabrese D, Heberer M, Gianni-Barrera R et al (2015) VEGF dose regulates vascular stabilization through Semaphorin3A and the Neuropilin-1⁺ monocyte/TGF-beta1 paracrine axis. *EMBO Mol Med* 7: 1366–1384
42. Wang HU, Chen ZF, Anderson DJ (1998) Molecular distinction and angiogenic interaction between embryonic arteries and veins revealed by ephrin-B2 and its receptor Eph-B4. *Cell* 93: 741–753
43. Wang Y, Nakayama M, Pitulescu ME, Schmidt TS, Bochenek ML, Sakakibara A, Adams S, Davy A, Deutsch U, Luthi U et al (2010) Ephrin-B2 controls VEGF-induced angiogenesis and lymphangiogenesis. *Nature* 465: 483–486
44. Erber R, Eichelsbacher U, Powajbo V, Korn T, Djonov V, Lin J, Hammes HP, Grobholz R, Ullrich A, Vajkoczy P (2006) EphB4 controls blood vascular morphogenesis during postnatal angiogenesis. *EMBO J* 25: 628–641
45. Meadows KN, Bryant P, Pumiglia K (2001) Vascular endothelial growth factor induction of the angiogenic phenotype requires Ras activation. *J Biol Chem* 276: 49289–49298
46. Simons M, Gordon E, Claesson-Welsh L (2016) Mechanisms and regulation of endothelial VEGF receptor signalling. *Nat Rev Mol Cell Biol* 17: 611–625
47. Sakurai Y, Ohgimoto K, Kataoka Y, Yoshida N, Shibuya M (2005) Essential role of Flk-1 (VEGF receptor 2) tyrosine residue 1173 in vasculogenesis in mice. *Proc Natl Acad Sci USA* 102: 1076–1081
48. Takahashi T, Yamaguchi S, Chida K, Shibuya M (2001) A single autophosphorylation site on KDR/Flk-1 is essential for VEGF-A-dependent activation of PLC-gamma and DNA synthesis in vascular endothelial cells. *EMBO J* 20: 2768–2778
49. Leitges M, Schmedt C, Guinamard R, Davoust J, Schaaf S, Stabel S, Tarakhovskiy A (1996) Immunodeficiency in protein kinase cbeta-deficient mice. *Science* 273: 788–791
50. Kawasaki J, Aegerter S, Fevurly RD, Mammoto A, Mammoto T, Sahin M, Mably JD, Fishman SJ, Chan J (2014) RASA1 functions in EPHB4 signaling pathway to suppress endothelial mTORC1 activity. *J Clin Invest* 124: 2774–2784
51. Kim I, Ryu YS, Kwak HJ, Ahn SY, Oh JL, Yancopoulos GD, Gale NW, Koh GY (2002) EphB ligand, ephrinB2, suppresses the VEGF- and angiopoietin 1-induced Ras/mitogen-activated protein kinase pathway in venous endothelial cells. *FASEB J* 16: 1126–1128
52. Martino MM, Brkic S, Bovo E, Burger M, Schaefer DJ, Wolff T, Gurke L, Briquez PS, Larsson HM, Gianni-Barrera R et al (2015) Extracellular matrix and growth factor engineering for controlled angiogenesis in regenerative medicine. *Front Bioeng Biotechnol* 3: 45
53. Lahteenvuo JE, Lahteenvuo MT, Kivela A, Rosenlew C, Falkevall A, Klar J, Heikura T, Rissanen TT, Vahakangas E, Korpisalo P et al (2009) Vascular endothelial growth factor-B induces myocardium-specific angiogenesis and arteriogenesis via vascular endothelial growth factor receptor-1- and neuropilin receptor-1-dependent mechanisms. *Circulation* 119: 845–856
54. Kivela R, Bry M, Robciuc MR, Rasanen M, Taavitsainen M, Silvola JM, Saraste A, Hulmi JJ, Anisimov A, Mayranpaa MI et al (2014) VEGF-B-induced vascular growth leads to metabolic reprogramming and ischemia resistance in the heart. *EMBO Mol Med* 6: 307–321
55. Bottinger EP, Factor VM, Tsang ML, Weatherbee JA, Kopp JB, Qian SW, Wakefield LM, Roberts AB, Thorgeirsson SS, Sporn MB (1996) The recombinant proregion of transforming growth factor beta1 (latency-associated peptide) inhibits active transforming growth factor beta1 in transgenic mice. *Proc Natl Acad Sci USA* 93: 5877–5882
56. Lin P, Polverini P, Dewhirst M, Shan S, Rao PS, Peters K (1997) Inhibition of tumor angiogenesis using a soluble receptor establishes a role for Tie2 in pathologic vascular growth. *J Clin Invest* 100: 2072–2078
57. He S, Kumar SR, Zhou P, Krasnoperov V, Ryan SJ, Gill PS, Hinton DR (2010) Soluble EphB4 inhibition of PDGF-induced RPE migration *in vitro*. *Invest Ophthalmol Vis Sci* 51: 543–552
58. Springer ML, Blau HM (1997) High-efficiency retroviral infection of primary myoblasts. *Somat Cell Mol Genet* 23: 203–209
59. Banfi A, Springer ML, Blau HM (2002) Myoblast-mediated gene transfer for therapeutic angiogenesis. *Methods Enzymol* 346: 145–157
60. Gu H, Cui M, Bai Y, Chen F, Ma K, Zhou C, Guo L (2010) Angiopoietin-1/Tie2 signaling pathway inhibits lipopolysaccharide-induced activation of RAW264.7 macrophage cells. *Biochem Biophys Res Commun* 392: 178–182
61. Zisch AH, Schenk U, Schense JC, Sakiyama-Elbert SE, Hubbell JA (2001) Covalently conjugated VEGF-fibrin matrices for endothelialization. *J Control Release* 72: 101–113
62. Kimura M, Kato Y, Sano D, Fujita K, Sakakibara A, Kondo N, Mikami Y, Tsukuda M (2009) Soluble form of ephrinB2 inhibits xenograft growth of squamous cell carcinoma of the head and neck. *Int J Oncol* 34: 321–327
63. Gianni-Barrera R, Burger M, Wolff T, Heberer M, Schaefer DJ, Gurke L, Mujagic E, Banfi A (2016) Long-term safety and stability of angiogenesis induced by balanced single-vector co-expression of PDGF-BB and VEGF164 in skeletal muscle. *Sci Rep* 6: 21546
64. Tsaryk R, Peters K, Barth S, Unger RE, Scharnweber D, Kirkpatrick CJ (2013) The role of oxidative stress in pro-inflammatory activation of human endothelial cells on Ti6Al4V alloy. *Biomaterials* 34: 8075–8085
65. Hamerlik P, Lathia JD, Rasmussen R, Wu Q, Bartkova J, Lee M, Moudry P, Bartek Jr J, Fischer W, Lukas J et al (2012) Autocrine VEGF-VEGFR2-Neuropilin-1 signaling promotes glioma stem-like cell viability and tumor growth. *J Exp Med* 209: 507–520
66. Rissanen TT, Korpisalo P, Karvinen H, Liimatainen T, Laidinen S, Grohn OH, Yla-Herttuala S (2008) High-resolution ultrasound perfusion imaging of therapeutic angiogenesis. *JACC Cardiovasc Imaging* 1: 83–91



License: This is an open access article under the terms of the Creative Commons Attribution-NonCommercial-NoDerivs 4.0 License, which permits use and distribution in any medium, provided the original work is properly cited, the use is non-commercial and no modifications or adaptations are made.